Thesis for The Degree of Licentiate of Engineering

Polymer brush functionalised nanopore sensors

Julia Järlebark

Department of Chemistry and Chemical Engineering
Chalmers University of Technology
Gothenburg, Sweden, 2024

Polymer brush functionalised nanopore sensors

Julia Järlebark

© Julia Järlebark, 2024
except where otherwise stated.
All rights reserved.

Technical Report No. 2024:03

Department of Chemistry and Chemical Engineering
Division of Applied Chemistry
Andreas Dahlin Group
Chalmers University of Technology
SE-412 96 Göteborg,
Sweden
Phone: +46(0)31 772 1000

Cover: Artistic representation of proteins translocating a polymer brush functionalised nanopore sensor.

Printed by Chalmers Digitaltryck,
Gothenburg, Sweden 2024.

Polymer brush functionalised nanopore sensors

Julia Järlebark

Department of Chemistry and Chemical Engineering
Chalmers University of Technology

Abstract

Single-molecule studies on proteins could reveal a lot of information about their conformational dynamics, and processes such as misfolding and aggregation. This knowledge is valuable in providing a deeper understanding of molecular biology, and for understanding the link between proteins and various diseases. Traditional averaging methods are unable to capture the dynamic behaviour and identify rare states within the protein population. However, conducting single molecule measurements on proteins presents inherent challenges, for instance limited observation time of the protein or, in an attempt to extend observation time, the tethering of proteins to a surface, potentially disturbing their delicate three-dimensional structure.

This thesis works towards the goal of developing a platform for long-term, non-intrusive single-molecule measurements on proteins. This is done by the integration of ionic current nanopore sensing with functional nanostructures. A novel nanochamber was fabricated through a combination of electron beam lithography, wet etching and controlled breakdown. This nanochamber, consisting of a cavity connected to two nanopores, is designed for protein trapping, where the nanopores would act as "gates".

Thus, the concept of macromolecular gating becomes central in protein trapping. The thesis demonstrates thermo-responsive gating for proteins using PNIPAM-functionalised nanopore arrays, as well as voltage-gating for both DNA and proteins with a PEG-functionalised single nanopore sensor. The utilisation of a voltage-gated nanopore allows for ion current readout, confirming molecular translocation through the pore. To facilitate nanopore sensing at higher voltages beyond the gating threshold, a Fourier transform-based algorithm for ion current data filtering has been developed.

Keywords

nanopore sensing, nanofabrication, polymer brushes

List of Publications

Appended publications

This thesis is based on the following publications:

[**Paper I**] Justas Svirelis, Zeynep Adali, Gustav Emilsson, Jesper Medin, John Andersson, Radhika Vattikunta, Mats Hulander, **Julia Järlebark**, Krzysztof Kolman, Oliver Olsson, Yusuke Sakiyama, Roderick Y. H. Lim, and Andreas Dahlin, *Stable trapping of multiple proteins at physiological conditions using nanoscale chambers with macromolecular gates*
Nature Communications 14 (Aug 2023)

Author contribution:
Fabricated the nanopore membranes.

[**Paper II**] John Andersson, **Julia Järlebark**, Sriram KK, Andreas Schaefer, Rebekah Hailes, Chonnipa Palasingh, Bagus Santoso, Van-Truc Vu, Chun-Jun Huang, Fredrik Westerlund, and Andreas Dahlin, *Polymer Brushes on Silica Nanostructures Prepared by Aminopropylsilatrane Click Chemistry: Superior Antifouling and Biofunctionality*
ACS Applied Materials & Interfaces (Feb 2023), 10228-10239

Author contribution:
Performed all the nanopore experiments. Co-authored the manuscript.

Other publications

The following publications were published during my PhD studies. However, they are not appended to this thesis, due to contents not closely related to the thesis.

[**a**] John Andersson, Justas Svirelis, Jesper Medin, **Julia Järlebark**, Rebekah Hailes, and Andreas Dahlin, *Pore performance: artificial nanoscale constructs that mimic the biomolecular transport of the nuclear pore complex*
Nanoscale Advances 4 23 (Sep 2022), 4925-4937.

[**b**] Vera Roth, **Julia Järlebark**, Alexander Ahrnens, Jens Nyberg, Justin Salminen, Teodora Retegan Vollmer, and Björn Wickman, *Mercury Removal from Concentrated Sulfuric Acid by Electrochemical Alloy Formation on Platinum*
ACS ES&T Engineering 2023 3 6 (Apr 2023) 823-830.

[**c**] Emma Feldt, **Julia Järlebark**, Vera Roth, Rasmus Svensson, Pontus K.G. Gustafsson, Nora Molander, Cristian Tunsu, and Björn Wickman, *Temperature and concentration dependence of the electrochemical $PtHg_4$ alloy formation for mercury decontamination*
Separation and Purification Technology 319 (May 2023).

Contents

Abstract i

List of Publications iii

I Summary 1

1 Introduction 3
1.1 Purpose . . . 5

2 Nanopore sensing 7
2.1 Nanopore sensing principle and terminology . . . 8
2.2 Nanopore conductance . . . 8
2.2.1 Access resistance . . . 10
2.2.2 Surface charge . . . 10
2.3 Molecular translocation through nanopores . . . 11
2.4 Electrophoresis and electroosmosis . . . 12
2.4.1 Electrophoretic force . . . 13
2.4.2 Electroosmotic flow . . . 13
2.4.3 Diffusion . . . 13
2.5 Capture rate . . . 13
2.6 Data acquisition and signal processing . . . 14
2.6.1 Signal filtering . . . 14

3 Polymer brushes 17
3.1 Polymers in solution . . . 18
3.1.1 The freely-jointed chain model . . . 18
3.1.2 Excluded volume and solvent interactions . . . 18
3.1.3 Lower critical solution temperature . . . 19
3.2 Modelling the structure of end-grafted polymer chains . . . 19
3.2.1 Polymer brushes on a curved surface . . . 20
3.3 Grafting of polymer brushes . . . 21
3.3.1 Poly(ethylene glycol) brushes . . . 22

4 Experimental **23**
4.1 Membrane fabrication 23
4.2 Chemicals 24
4.3 Nanopore fabrication by controlled breakdown 25
4.3.1 Experimental setup 25
4.3.2 Nanopore fabrication 25
4.3.3 Nanopore conditioning 26
4.4 Ion current measurements 27

5 Nanofabrication: Nanoscale structures suitable for protein trapping and gating **29**
5.1 Paper I: Nanopores for protein gating 29
5.1.1 Fabrication of nanopore arrays 29
5.1.2 Protein gating in nanopores by thermo-responsive polymer brushes 31
5.2 Unpublished results: Nanochambers for protein trapping 32
5.2.1 Nanochamber fabrication 32
5.2.2 Electrical characterisation 33

6 Data analysis: Enabling high-voltage nanopore recordings **37**
6.1 Low- and high-pass filtering of nanopore data 37
6.2 Data analysis example 38

7 Towards a voltage-gated nanopore **39**
7.1 Paper II: Functionalised SiN nanopores 39
7.1.1 Grafting of PEG brushes to silica surfaces 39
7.1.2 PEG grafting on SiN nanopores 40
7.2 Unpublished results: Molecular translocation through functionalised nanopores 41

8 Conclusion and future work **43**

Acknowledgements **44**

Bibliography **45**

II Appended Papers **50**

Part I

Summary

Chapter 1

Introduction

The field of nanotechnology can be traced back to Richard Feynman's influential lecture, "There is plenty of room at the bottom", wherein he laid the conceptual foundation for the miniaturisation of objects, ranging from books to electrical motors.[1] Feynman envisioned an entire field of physics dedicated to manipulating matter at the atomic scale, and today, nanotechnology stands as a rapidly evolving interdisciplinary research field between physics, chemistry and biology. The impact of nanotechnology cannot be overstated, with applications in diverse areas, including biomedicine, food industry, computer science, informatics to environmental sciences and energy production.[2] Over the past 65 years since Feynman's lecture, the remarkable progress in nanotechnology has transformed the theoretical vision into reality, facilitating the miniaturisation of various objects. This thesis aligns well with this vision, as it is concerned with the miniaturisation of items such as "cages" and "doors".

These miniaturised versions of cages and doors would be tailored towards proteins, enabling more detailed investigations than are currently feasible. However, before delving into technical details, let's explore the motivation behind studying proteins. In living organisms, nucleic acids handle information storage, while most functions are governed by proteins. They catalyse chemical reactions as enzymes, provide structural support like collagen, and facilitate communication between cells through hormones. Consequently, proteins stand as the fundamental building blocks of life. In contrast to our profound understanding of matter, built upon the study of atoms as its fundamental constituents, our current comprehension of the origin and essence of life remains incomplete. Thus, the investigation of properties and behaviour of proteins could help us move towards a deeper understanding of biology and life.

On a more applied note, protein malfunction is a prevalent factor in numerous diseases. Proteins are large polymeric biomolecules folded into a three-dimensional structure based on the amino acid sequence. It is noteworthy that there are also a number of proteins, known as intrinsically disordered proteins, that do not have a definite, well-defined, three-dimensional structure and instead switch between different conformational states. The three-dimensional structure, including the structural flexibility in the case of intrinsically dis-

ordered proteins, plays a decisive role in determining the biological function of the protein.[3] As such, a disturbance in the structure of the protein can lead to an altered function of the protein. As an example, the misfolding of proteins and their subsequent aggregation into expansive, ordered structures known as amyloids is linked to many neurodegenerative diseases like Alzheimer's disease and Parkinson's disease. Despite being a forefront topic in current research, the aggregation process and its direct link to these diseases remain incompletely understood.[4] Gaining a deeper understanding of protein dynamics, interactions and aggregation could not only contribute to answering the fundamental questions about life, but also advance research aimed at understanding and addressing the causes and potential treatments for such diseases.

To investigate dynamic processes in detail, it is essential to avoid averaging over time or the number of molecules. There is in general no synchronisation of molecular dynamics, which makes it difficult to capture dynamic behaviour by averaging across a large population of molecules. Thus, a single-molecule technique stands out as the most fitting choice. Moreover, the conventional averaging approach risks overlooking rare states in the population that might not significantly contribute to the average. Concerning time averaging, the time scales for these processes span from submicroseconds to minutes/hours.[3] Hence, it becomes crucial to consider both the time resolution of the technique, to capture rapid conformational transitions, and the potential length of the measurement to thoroughly investigate the often slower protein misfolding and aggregation processes.

Several single-molecule techniques have already been employed to study protein dynamics, including fluorescence microscopy methods like Förster Resonance Energy Transfer (FRET), force spectroscopy techniques such as Atomic Force Microscopy (AFM), and nanopore sensing with ion current readout. While fluorescence microscopy can achieve high temporal resolution down to nanoseconds, its drawback lies in typically short observation times (milliseconds), unless the analyte is immobilised on a surface. Tethering the protein to a substrate, a requirement also for force spectroscopy, can potentially interfere with the protein's native structure and function.[3] Nanopore sensing, on the other hand, offers high temporal resolution (down to tens of nanoseconds, depending on the bandwidth of the instrumentation), though observation times are typically limited to the translocation time of the analyte, typically in the microsecond regime.[5]

Using the above-mentioned methods, it is possible to perform interesting studies and provide some insight into protein dynamics, however there is to the best of my knowledge no technology available that is capable of:

- Single molecule measurements on proteins
- Long-time measurement (ideally hours, at least minutes)
- Non-intrusive towards proteins

We now return to the idea that was introduced in the beginning of this chapter, with miniaturised cages and doors for proteins. One strategy to achieve the goal of developing a method as described above involves trapping the

protein inside a closed nanostructure. Ideally, the loading of protein(s) into the nanostructure should be controlled, to precisely determine the number of trapped proteins. During measurement, no external forces should be applied to the protein to avoid any risk of interfering with its native conformation(s). Additionally, it is essential that proteins cannot escape from the trap during the experiment. Therefore, the inclusion of a gate mechanism is necessary for proteins to enter the nanosized trap. Polymer brushes have emerged as promising candidates for macromolecular gating. Various gating mechanisms, including pH, temperature, and solvent responsiveness, as well as molecular recognition, have been demonstrated.[6]–[8] A drawback of these methods is the absence of a definitive readout to confirm the number of molecules that have passed through the gate. However, ionic current readout offers the capability to count the number of molecules translocating through a single nanopore. This led to the hypothesis that a polymer brush functionalized nanopore could serve as a macromolecular gating system controlled by voltage, with ionic current readout providing confirmation of molecular translocation through the gate.

1.1 Purpose

This thesis aims to progress towards the goal of developing a platform for studying single protein dynamics through the integration of nanopore sensing with functional nanostructures. More precisely, the research included in this thesis is:

- Fabrication and characterisation of nanostructures (nanopores and nanochambers) suitable for trapping and gating of proteins.
- Development of an algorithm that enables nanopore sensing at higher voltages.
- Investigations of the functionalisation of nanopore sensors with polymer brushes.
- Preliminary results indicating a voltage-gated behaviour observed in polymer brush functionalised nanopores, towards both DNA molecules and proteins.

Through these research components, this thesis strives to lay the groundwork for a platform that enables controlled and non-intrusive measurements of single protein dynamics over relevant time-scales.

Chapter 2

Nanopore sensing

The concept of utilising variations in the electrical current through a small hole for particle sensing purposes dates back to 1948, when Wallace H. Coulter demonstrated counting of individual blood cells through this technique, a method still extensively used in current cell counting technology. The Coulter principle is based on monitoring the electrical current through a micrometer-sized aperture. When a particle of similar dimensions, such as a cell, passes through the aperture, it induces a transient change in the measured current, thus enabling the counting of individual particles.[9]

A nanopore sensor employs the same fundamental principle as the Coulter counter, however at the nanoscale. Consequently, the currents in a single nanopore measurement are extremely small, typically ranging from pico- to nanoamperes. The recording of such microscopic currents is a well-established practice in electrophysiology; Erwin Neher and Bert Sakmann were awarded the Nobel Prize in Physiology or Medicine in 1991 for their development of the extracellular patch-clamp technique, which allowed the precise recording of current through single ion channels in the cell membrane.[10],[11]

The foundation of nanopore sensing can be said to have originated with the basic idea proposed by David Deamer in 1989. Deamer hypothesised that it should, in principle, be possible to distinguish the different nucleobases of DNA as they pass through a narrow channel.[12]–[14] Throughout the 1990s, this idea was experimentally investigated, leading to the detection of the first DNA and RNA strands using the biological α-hemolysin pore embedded in a lipid bilayer.[15] Subsequent refinement of the technique has made it possible to identify the individual nucleobases, and the technique has since been commercialised by Oxford Nanopore for DNA sequencing.[12]

Undoubtedly, the prospect of using nanopores for nucleic acid sequencing, and nowadays for protein and peptide sequencing, has been the major driving force in the development of nanopore sensing technologies. However in the meantime, also many other interesting applications of single nanopore sensors have been explored and developed. Various types of nanopores have been employed, including a wide variety of biological pores (such as the α-hemolysin), solid-state pores in conventional silicon-based materials and novel 2D materials.

Hybrid pores, composed of a biological pore inserted into a solid-state pore, have also been investigated.[13],[14] These nanopore sensors have been used to detect various analytes, including DNA, RNA, proteins, peptides, and other biomolecules. Despite all the progress made, challenges such as low selectivity, high noise (see Section 2.6.1), frequent clogging of molecules in the nanopore (discussed in Chapter 7) and limited observation time of the molecule inside the pore still remain to be solved.[14]

The remainder of this chapter aims to introduce the fundamental principle of nanopore sensors, and then go more into detail on the physics governing molecular transport through nanopores. Note that the focus will be exclusively on solid-state pores, in accordance with the scope of this thesis.

2.1 Nanopore sensing principle and terminology

This section covers the fundamental principles of nanopore sensing by ion current measurements, aiming to familiarise readers with essential concepts and terminology commonly employed in the field. The setup of a typical single nanopore experiment is illustrated in the left panel of Figure 2.1a). A thin membrane acts as the sole chemical and electrical connection between two liquid reservoirs. These reservoirs are filled with electrolyte buffer (typically 1 M KCl), and equipped with electrodes, commonly Ag/AgCl. Applying a constant voltage bias ΔV across the electrodes initiates the flow of ions (K^+ and Cl^-) through the nanopore, resulting in the generation of an ionic current, the *open-pore current* I_0. The right panel of Figure 2.1a) illustrates the measurable ionic current.

In a sensing experiment, molecules (generally referred to as *analytes*) are introduced to the *cis* side of the membrane. The *translocation* of an analyte across the nanopore to the *trans* side is registered as a transient decrease in the ionic current, as depicted in Figure 2.1b). The translocation *event* is characterised by its *dwell time* τ (i.e. the molecule's residence time inside the pore), its *blockage amplitude* ΔI and, in certain cases, its number of *levels*. An event may exhibit multiple levels if the analyte is not a homogeneous linear polymer, or does not pass through the pore in a straight linear fashion. For instance, a partially folded DNA strand can produce a multi-level event. Various factors may contribute to the blockage current, with a basic model suggesting that the reduction in current stems only from the fact that the volume occupied by the analyte cannot be simultaneously occupied by ions.[14],[16] Molecular translocations and related physical phenomena will be discussed more in detail in Sections 2.3 and 2.4.

2.2 Nanopore conductance

A solid-state nanopore typically exhibits linear, ohmic (resistor-like) I-V characteristics at voltages below ~ 1 V,[16] as illustrated in Figure 2.2a). However, non-linear (diode-like) I-V characteristics, as seen in Figure 2.2b), can also be observed. This is a phenomenon known as ion current rectification, which

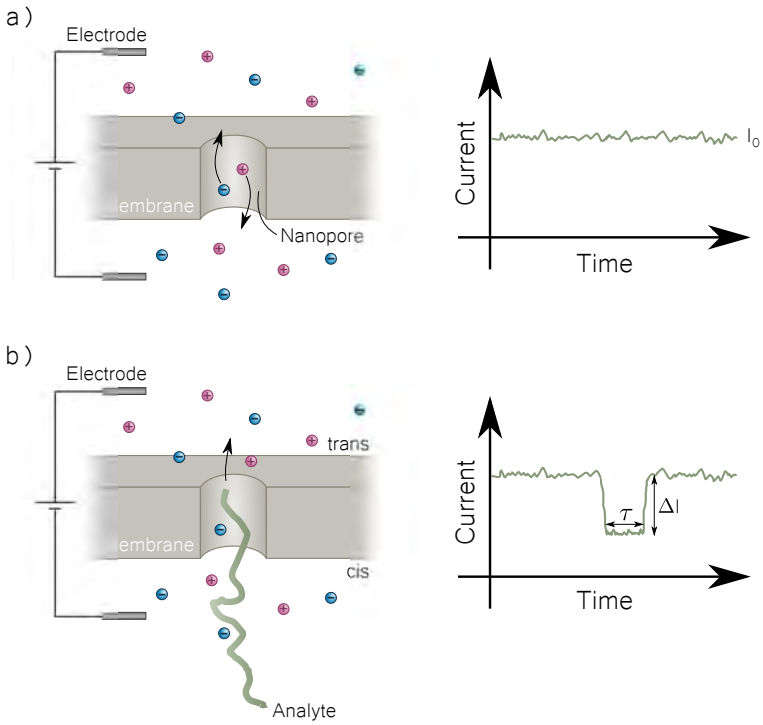

Figure 2.1: The nanopore sensing principle. a) A solid-state nanopore embedded in a thin membrane, with a corresponding baseline ionic current I_0 due to a transmembrane potential applied between the electrodes. b) Introduction of an analyte on the cis side results in the detection of an event in the ionic current when the molecule translocates the nanopore. The dwell time τ corresponds to the residence time of the molecule inside the pore, and the blockage amplitude ΔI represents the decrease in current caused by the analyte.

is related to some asymmetry in the nanopore, either in the geometry or the surface charge of the pore walls.[17]

We will begin by modelling the nanopore conductance for a narrow, cylindrical nanopore at high ionic strength (high salt concentration), and then discuss the refinements needed to generalise the model to other conditions. Our initial model considers the nanopore resistance to depend solely on pore geometry. The shape of a solid-state pore is determined by its fabrication method. Nanopores used in this thesis are fabricated by either electron beam lithography (EBL) and reactive ion etching (RIE) or controlled breakdown (CBD), described more in detail in Chapter 4. Nanopores fabricated by EBL and RIE are, to a very high degree, cylindrical.[18],[19] Also for CBD pores, a cylindrical model correlates well with experimental data.[20],[21]

It can be reasoned that the conductance $G = \frac{I_0}{\Delta V}$ must then be proportional to the bulk conductivity σ of the electrolyte and the cross-sectional area of the nanopore, and inversely proportional to the length of the pore (equivalent to

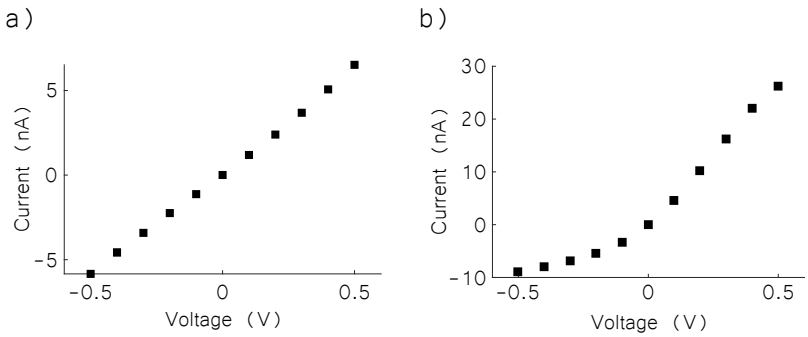

Figure 2.2: I-V curves recorded for two different solid state nanopores; a) showing linear, ohmic behaviour, and b) showing non-linear, rectifying behaviour.

the membrane thickness t in the case of a cylindrical pore). This gives

$$G = \sigma \frac{\pi d^2}{4t} \tag{2.1}$$

where d is the nanopore diameter.

2.2.1 Access resistance

The model presented works well for $d < t$, but for wider pores, when $d \gtrsim t$, the model breaks down.[22] The reason is that the model considers only the resistance of the pore itself, assuming that the entire potential drop occurs across the nanopore. However, in reality, there is also access resistance - the resistance the current encounters as it enters or exits the pore. A more accurate electrical circuit model of the nanopore setup is shown in Figure 2.3. This model includes the capacitance and resistance of the supporting chip, the membrane capacitance, the electrolyte resistance, as well as the two access resistances. The commonly accepted value of the access resistance of a nanopore is $\frac{1}{2d\sigma}$.[22],[23] Including this effect into equation 2.1, we obtain

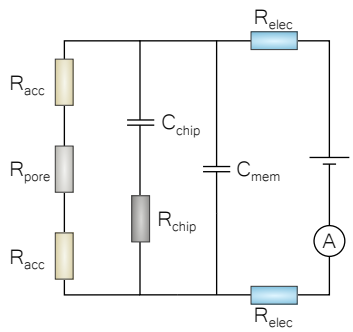

Figure 2.3: Electrical circuit model for the nanopore sensing setup, including the chip capacitance and resistance, the membrane capacitance, the electrolyte resistance and the two access resistances.

$$G = \sigma \left(\frac{4t}{\pi d^2} + \frac{1}{d} \right)^{-1} \tag{2.2}$$

2.2.2 Surface charge

To accurately model nanopore conductance, surface effects must be considered. This section will be limited to silicon nitride pores, the most common type of

solid state pores, and the focus of this thesis. Silicon nitride surfaces undergo rapid oxidation in air, forming a surface chemistry consisting of silanol (SiOH) groups and unoxidized primary amine sites ($SiNH_2$). Amine sites can carry a positive charge (NH_3^+) and has a pK_a of about 10, while silanol groups can be either positively or negatively charged ($SiO^-/SiOH_2^+$) with a $pK_a \sim 2$.[24],[25] Thus, the surface charge of silicon nitride nanopore walls depends on pH and the ratio between amine sites and silanol groups. Measurements of the zeta potential indicate a negative surface charge above ∼pH 5 and a positive charge below that value.[25]

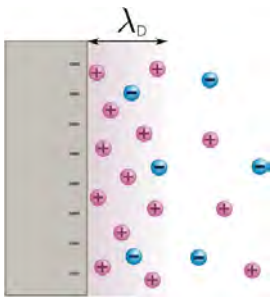

Figure 2.4: The negative surface charge is screened by an electric double layer.

Charged surfaces in solution are screened by the accumulation of oppositely charged counter-ions (primarily K^+ ions in the case of negatively charged silicon nitride) close to the surface, as illustrated in Figure 2.4. This phenomenon is known as an electric double layer (EDL), forming a diffuse cloud of both counter- and co-ions. The extension of the EDL from the surface is known as the Debye length (λ_D), and depends on the ionic strength of the electrolyte. At high salt concentrations $\sim$ 1 M, $\lambda_D \approx 0.3$ nm, while it extends further at lower salt concentrations. The nanopore conductance increases due to the accumulation of ions at the silicon nitride surface inside the pore. While at high ionic strength, this effect may not be measurable, at low salt concentrations ($\lesssim$ 100 mM), it results in a higher conductance of the nanopore than would be anticipated solely from the bulk contribution of K^+ and Cl^- ions.

2.3 Molecular translocation through nanopores

With a solid understanding of nanopore conductance in the absence of an analyte, this section deals with how the introduction of an analyte impacts nanopore conductance. As a first approximation, it can be assumed that the reduction in conductance is solely attributed to the exclusion of ions from the volume occupied by the analyte, reducing the number of available charge carriers for ionic conductance. This assumption yields the following expression:

$$\Delta G = \sigma \frac{\pi d_{\text{analyte}}^2}{4t} \tag{2.3}$$

This model is also based on the assumption that the analyte is approximately cylindrical and longer than the pore length, as illustrated in Figure 2.5a).[26]

This basic model proposes that the blockage amplitude depends solely on the cross-sectional area of the analyte, however it also varies with pore size.[22] A more precise model, accounting for pore size dependence, should incorporate access resistance, which dominates in wider pores. The impact of an analyte on nanopore conductance for a cylindrical analyte (e.g. a DNA

strand translocating in a linear state) can then be calculated based on insertion into equation 2.2, which gives

$$\begin{aligned}\Delta G &= G_0 - G_{\text{analyte}} \\ &= \sigma \left(\left(\frac{4t}{\pi d^2} + \frac{1}{d} \right)^{-1} - \left(\frac{4t}{\pi (d^2 - d_{\text{analyte}}^2)} + \frac{1}{\sqrt{d^2 - d_{\text{analyte}}^2}} \right)^{-1} \right)\end{aligned} \tag{2.4}$$

For a spherical analyte (such as a protein or coiled DNA during translocation) as shown in Figure 2.5b), the conductance blockage is given by[27]

$$\Delta G = \sigma \frac{\pi d^2 \left(d^2 - d_{\text{analyte}}^2 \right)}{4 \left(d_{\text{analyte}}^3 + t d^2 - t d_{\text{analyte}}^2 \right)} \tag{2.5}$$

Furthermore, for highly charged analytes such as DNA, it is important to consider charge screening. As the analyte translocates the pore, it carries a layer of counter-ions, thus increasing the number of available charge carriers for ionic conductance. This effect counteracts the volume exclusion effect described earlier. At high salt concentrations, the volume blocking effect dominates, causing a decrease in current during translocation. However, at low salt concentrations, the increase of charge carriers in the analyte EDL dominates, and results in a current enhancement during the event.[28],[29]

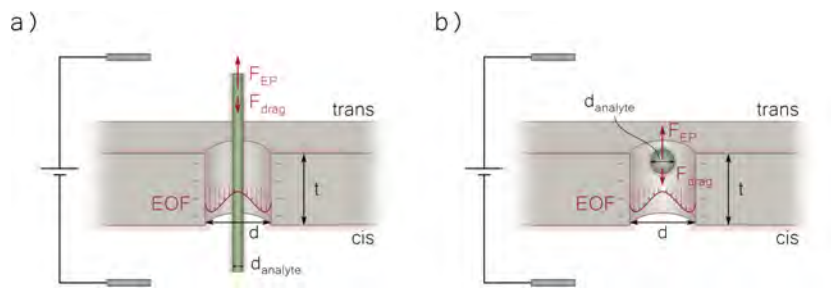

Figure 2.5: Schematic illustrating the model for translocation of a) a cylindrical analyte and b) a spherical analyte. The diagram shows both electrophoretic and drag forces, along with electroosmotic flow.[30] The assumption in this figure (affecting the direction of forces) is that both the nanopore walls and the analyte are negatively charged.

2.4 Electrophoresis and electroosmosis

So, what is it then that makes the analyte move through the nanopore? This is an interplay between electrophoretic forces, electroosmotic flow and diffusion, and the impact of these effects depends on pH, ionic strength and the type of analyte.

2.4.1 Electrophoretic force

When a voltage bias is applied across a nanopore, this sets up an electric field inside, and close to, the nanopore. This electric field can be very strong, up to $\sim 10^7$ V/m. The electrostatic force from this field on a charged analyte is the origin of electrophoretic transport, which is the main driving force for translocation of highly charged analytes, such as DNA molecules. For the case in Figure 2.5a), where DNA is modelled as a cylindrical analyte longer than the pore, and with a uniformly distributed line charge density λ_{DNA}, the electrophoretic force is $F_{\text{EP}} = \lambda_{\text{DNA}}\Delta V$. The resulting force will however be less than this, because the counter-ions associated with the analyte will be affected by an opposing electrostatic force from the electric field, creating a drag force which counteracts the electrophoretic force on the analyte.[31]

2.4.2 Electroosmotic flow

Electroosmosis is an effect observed in micro- and nanofluidic channels, such as nanopores, under the influence of an external electric field. As discussed earlier, counter-ions accumulate in an EDL near the nanopore walls (within λ_D). When the electric field acts on this charged layer, it induces a flow inside the channel as the ions drag along the solution, a phenomenon known as electroosmotic flow (EOF), illustrated in Figure 2.5. The velocity profile will depend on the ratio between λ_D and d, i.e. on the ionic strength of the electrolyte.[27],[30] It also depends on the aspect ratio of the nanopore; in long micro- and nanofluidic channels the EOF profile is known to be plug-like, while in nanopores the flow is higher close to the pore walls.[30]

The electroosmotic flow exerts a force on the analyte, thereby influencing its translocation behaviour. The direction of this force can be either parallel or opposite to that of the electrophoretic force, depending on the relative charge of the analyte and the nanopore walls. If the pore walls and the analyte have the same charge, the electroosmotic flow opposes the electrophoretic force. Conversely, if the pore walls have an opposite charge to the analyte, electroosmotic flow aligns with the electrophoretic force.[25],[32]

2.4.3 Diffusion

In addition to electrophoresis and electroosmosis, the diffusion or random walk of the analyte in solution is always present, and unaffected by applied voltage. Diffusion is driven by the concentration gradient of the analyte between the cis and trans chambers. Notably, protein translocation via diffusion has been observed, when electrophoretic and electroosmotic effects counterbalance each other.[25]

2.5 Capture rate

Another important parameter in nanopore sensing is the *capture rate* or event frequency, representing the number of observed events per unit time. The

movement of a free molecule in solution is governed by diffusion, when the analyte is distant from the nanopore opening. However, within the "capture zone", the analyte's movement is dominated by the electric field. To enter the pore, the analyte must first diffuse close enough to the pore, where it can be captured by the electric field, and then translocate through the nanopore. Consequently, two potential rate-determining steps exist in the capture process.

In the case where the pore is significantly larger than the analyte ($d >> d_{\text{analyte}}$), there should be no barrier towards translocation, and the capture rate is expected to be determined by the analyte's diffusion to the "capture zone". The radius of this capture zone increases linearly with voltage, implying that the event frequency should be proportional to ΔV in cases of a diffusion-limited process. This behaviour has been observed in DNA translocation through nanopores that are large (~ 15 nm) compared to the DNA cross-section.[26],[33]

On the other hand, in situations where a barrier to translocation exists, such as when the pore size is small compared to the analyte, requiring conformational changes for entry, molecules are delivered to the pore faster than they can translocate it. In this case, with a barrier to overcome, the capture rate is expected to follow an exponential dependence on ΔV. This behaviour has been observed for the translocation of DNA in the 100-1000s bp range through small (< 5 nm) pores.[33]

2.6 Data acquisition and signal processing

We now move on to the process of acquiring ionic current data in nanopore sensing experiments. The ionic current signal we record is a continuous, *analog* representation. To enable storage and computerised processing, it must be converted into a discrete, *digital* signal through a procedure known as *sampling*. The chosen sampling rate determines the time resolution of the experiment. According to the Nyquist sampling theorem, the sampling interval T_s required for accurate reconstruction of a signal containing important information up to the frequency f_x is given by:

$$T_s = \frac{1}{2f_x} \tag{2.6}$$

With this sampling interval, the signal can be perfectly reconstructed up to frequencies f_x.[34] Thus, the highest achievable bandwidth is determined by the sampling rate. However, it's essential to note that in practice, the bandwidth of the nanopore recording will usually be reduced due to the need for signal filtering.

2.6.1 Signal filtering

One of the main challenges in the development of solid-state nanopore sensors is the low signal-to-noise (SNR) ratios. Noise can originate from various sources. High-frequency noise is often linked to chip capacitance (see Figure 2.3). Low-frequency noise typically scales as $\frac{1}{f}$ and is thought to be associated with nanopore surface properties, including surface charge, hydrophobicity, and the

presence of nanobubbles. To enhance the SNR, the signal is frequently filtered before and/or after sampling. An analog filter consists of an electrical circuit and operates on the analog signal, while a digital filter is a mathematical operation applied to the digitised signal. In nanopore measurements, the most commonly used filter is a low-pass filter, which eliminates frequency components higher than a specified *cut-off frequency* f_c. While this improves the SNR, it comes at the cost of temporal resolution. This means that the most rapid processes in the data may no longer be possible to observe.[35],[36]

Chapter 3

Polymer brushes

Surface functionalisation is a growing topic within a wide range of biotechnological applications, including biomedicical devices and biosensors. Surface modification is often employed to achieve surfaces with anti-fouling properties, preventing unwanted, non-specific interactions between the surface and biomolecules.[37] Additionally, there may be a need to modify and tailor interactions with molecules. One type of surface functionalisation that has attracted significant interest in recent years is polymer brushes.

In the field of nanopore sensing, surface modification can potentially play an important role, due to its ability to influence the interactions between the nanopore and the analyte.[14],[38] This includes preventing nanopore clogging by reducing analyte-surface interactions, or achieving nanopore selectivity. Modifying the nanopore surface chemistry can also impact electroosmotic flow, the ion current rectification (via alterations to the surface charge density of nanopore walls), and analyte residence time in the pore.[14],[38]

Given the many possibilities for tuning nanopore properties, various methods for surface functionalisation have been explored. Current common techniques include dressing the nanopore with a lipid bilayer, surfactant adsorption, self-assembled monolayers, and silanisation chemistry.[38] While there are also some notable examples of employing different polymeric coatings in solid-state nanopore sensors,[39]–[41] this remains a relatively unexplored area. For instance, the effects of polymer brushes grafted inside solid-state nanopore sensors on properties such as ionic current, noise and molecular translocation remains unknown.

This thesis investigates precisely this - the chemical functionalisation of nanopore sensors with polymer brushes. This chapter serves to establish the theoretical foundation for polymer brushes. We begin with modelling free polymers in solution, and then move on to polymers that are attached to a surface. Different grafting strategies are discussed, with a particular focus on poly(ethylene glycol).

3.1 Polymers in solution

A polymer is a large macromolecule composed of smaller units known as monomers, that are covalently linked together. The polymer chain architecture may be linear or branched. However, for the purpose of this chapter, the focus is on linear polymers and their behaviour in solution.

3.1.1 The freely-jointed chain model

A polymer in solution can be viewed as a flexible chain, consisting of n segments, each with a length l. In this view, l represents the monomer length and n is the number of monomers. The flexibility of a polymer allows for various conformations, typically adopting a random coiled structure. One way to model the random coil is through the freely-jointed chain model, which assumes that the polymer is constructed by connecting the segments to each other using a random-walk, allowing an arbitrary angle α between each segment (see Figure 3.1).[42]

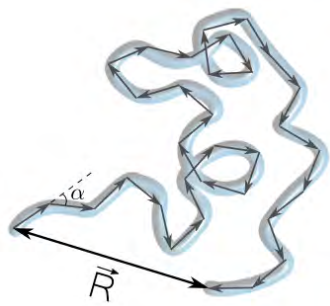

Figure 3.1: The freely-jointed chain model for a polymer in solution.

However, the assumption of an arbitrary angle α between segments is not so realistic, especially for stiffer polymers. To address the varying flexibility among polymers, the *Kuhn length* l_k is introduced into the model. According to Kuhn, the polymer can instead be seen as composed of n_k segments, each of length l_k, resulting in a total length, or *contour length* L, expressed as $L = nl = n_k l_k$.[42] For highly flexible polymers, $l_k \Rightarrow l$, while for rigid, rod-like polymers $l_k \Rightarrow L$.

In the freely-jointed chain model, the *mean end-to-end distance* $\langle R \rangle$ provides a common measure to describe the size of a polymer coil. It is given by[42]

$$\langle R \rangle = \left(n_k l_k^2\right)^{\frac{1}{2}} = (nll_k)^{\frac{1}{2}} \tag{3.1}$$

An even more physically relevant measure of the coil size is (twice) the *radius of gyration* $2R_g$, calculated as the root mean square distance of the segments from the centre of mass. It is related to the mean end-to-end distance as $R_g = \frac{1}{\sqrt{6}}\langle R \rangle$.[43] Note that both the end-to-end distance and the radius of gyration have the same scaling relationship with the polymer length, $n^{\frac{1}{2}}$.

3.1.2 Excluded volume and solvent interactions

The freely-jointed chain model can be refined by including the effects of excluded volume and solvent interactions, which is done in the Flory-Huggins theory for polymers in solution.[43] Firstly, the excluded volume effect means that two different polymer segments cannot simultaneously occupy the same volume space, leading to a reduction in the available volume compared to the simple

freely-jointed chain model. Additionally, the interactions between the polymer and the solvent, as well as among solvent molecules and between different parts of the polymer chain, must be considered. The relative strength of these interactions significantly influences the polymer size in solution, leading to a revised scaling relationship for the polymer coil size[43]

$$2R_g \sim n^{\frac{3}{5}} \tag{3.2}$$

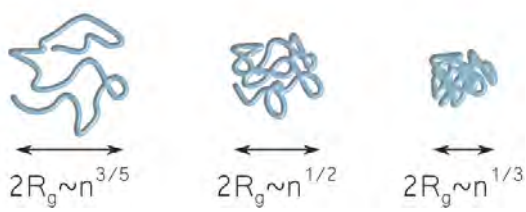

Figure 3.2: The size and shape of a polymer coil in different solvent conditions.

Three distinct cases can be identified, depending on the relative strength of the polymer-polymer, solvent-solvent and polymer-solvent interactions, also illustrated in Figure 3.2:[42]

- Good solvent ⇒ The polymer coil swells and the size scales as $2R_g \sim n^{\frac{3}{5}}$
- θ solvent ⇒ The excluded volume effect and solvent interactions counter-balance each other, so that the polymer follows the freely-jointed model, with the scaling $2R_g \sim n^{\frac{1}{2}}$
- Poor solvent ⇒ The polymer contracts into a globule to avoid interaction with the solvent, resulting in a size scaling of $2R_g \sim n^{\frac{1}{3}}$

To summarise, the size of the polymer coil is highly dependent on the solvent conditions, which is an important consideration in the preparation of polymer brushes.

3.1.3 Lower critical solution temperature

The solubility of a polymer in a certain solvent depends also on temperature, and, in fact, for some polymers, the solubility decreases with temperature. That means, there exists a temperature such that the polymer is soluble below, but insoluble above. This temperature is known as the *lower critical solution temperature* (LCST) of the polymer.[42]

3.2 Modelling the structure of end-grafted polymer chains

We now shift our focus to the central theme of this chapter: surface functionalisation with polymer brushes. While there are different ways polymers can

interact with a surface, we only consider polymers attached with one end to the surface, so called *end-grafting*. The conformation these end-grafted polymers assume (illustrated in Figure 3.3) is determined by the the *grafting density* Γ of the polymers on the surface and the nature of interactions between the polymer chain and the surface. At low grafting densities $\Gamma \lesssim \frac{1}{R_g^2}$, the *mushroom* or *pancake* conformations are possible.[43] The pancake structure is observed when attractive interactions between the polymer chain and the surface favour adsorption. Conversely, the mushroom conformation occurs when polymer-surface interactions are unfavourable. The pancake structure has very limited extension from the surface, while the mushroom extends approximately $2R_g$ from the surface.[43]

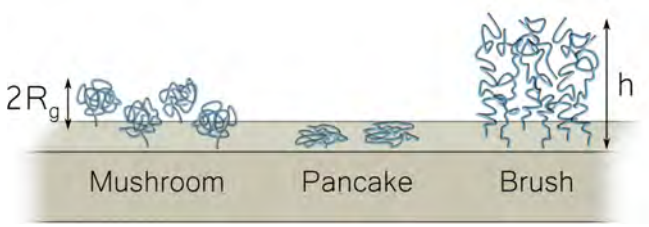

Figure 3.3: Different conformations of polymers that are end-grafted to a surface. At low grafting densities, "pancakes" or "mushrooms" are produced, while at high grafting densities, stretched "brushes" result.

For high grafting densities $\Gamma > \frac{1}{r^2}$, there is not enough space for the polymers to adopt a mushroom configuration. Instead, they are forced to stretch out in solution, forming what is known as a *polymer brush*. The extension of the brush is, of course, dependent on the grafting density and the solvent conditions. In the case of a good solvent, the Alexander - de Gennes theory provides a scaling relation for the polymer brush height h:[43]–[45]

$$h \sim n\Gamma^{\frac{1}{3}} \tag{3.3}$$

This is in contrast to the coil size $2R_g$ that scales as $n^{\frac{3}{5}}$. In the Alexander - de Gennes theory, the volume fraction of monomers $\phi(z)$ as a function of distance from the surface, is assumed to follow a step-function, with a constant value for $z < h$ and 0 for $z > h$. More sophisticated models based on self-consistent field theory have estimated the volume fraction to instead follow a parabolic density profile, where the monomer concentration gradually decreases as one moves away from the surface.[46]

3.2.1 Polymer brushes on a curved surface

This is all concerned with polymer brushes grafted on planar surfaces. As this thesis deals with polymer brushes grafted inside of nanopores, it is also relevant to consider how a curved surface affects the brush architecture. A polymer brush grafted on a concavely curved surface (such as the inside of a nanopore), will have an extension $H > h$, where h is the height for the same

brush on a planar surface.[47],[48] This can easily be understood by considering that the volume available for the monomers will be less, and thus, the brush will be forced to stretch further out in solution. The brush height H inside the nanopore will therefore be a function of the curvature, extending further from the surface as the curvature increases. This is valid as long as $H < \frac{d}{2}$, that is, when there is still a channel of free solution in the middle of the pore, where $\phi(r > H) = 0$. When the curvature increases further, a limit will be reached when the entire pore volume is filled with the (hydrated) brush, that means that $\phi(r) > 0$ everywhere inside the pore. After this, with further increases in curvature, the brush will be compressed.[47],[48] Both of these cases are illustrated in Figure 3.4.

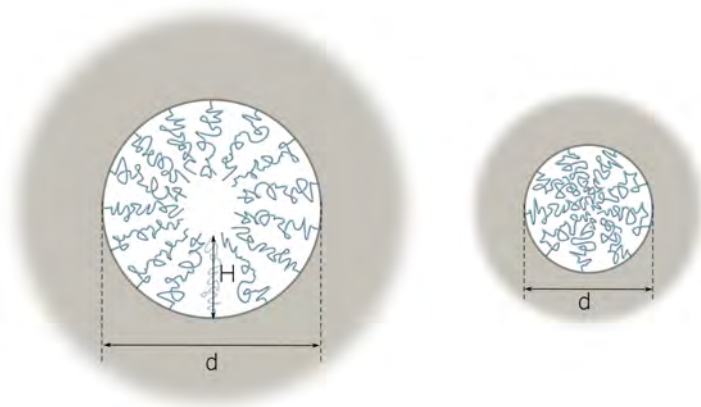

Figure 3.4: Schematic of polymer brushes grafted inside a nanopore. For large pores (compared to the brush height) there will be a hollow channel in the pore centre. In the case of smaller pores, the brush will be compressed and fill up the entire pore volume.

3.3 Grafting of polymer brushes

In general, there are two primary methods for forming a polymer brush: *grafting-to* and *grafting-from*.[45] In the grafting-from approach, brushes are prepared by functionalising the surface with an initiator layer, followed by a surface initiated polymerisation reaction from monomers in solution. This method offers advantages such as high grafting density and tunable polymer brush thickness. However, the method is not so realistically applicable in a diverse field such as nanopore sensing, as it lacks in experimental simplicity and accessibility for researchers outside of the field of organic chemistry.

This project instead employs the grafting-to method, which is experimentally very straight-forward. In this method, polymers in solution are attached by one end to the surface. This requires a functional end group on the polymer capable of binding to the surface. However due to steric hindrance between the

polymers during surface binding, achieving high grafting densities and reaching the "strongly stretched" brush regime can be challenging.[37],[45]

3.3.1 Poly(ethylene glycol) brushes

The purpose of surface functionalisation of nanopores in this thesis is mainly to investigate the prospects for trying to create a voltage-gated nanopore. Poly(ethylene glycol) (PEG) is chosen as the polymer for this purpose, as it is known to form an entropic barrier towards spontaneous (diffusive) protein translocation in larger nanopores.[6] PEG is also known for its anti-fouling properties, preventing non-specific adsorption to surfaces.[37],[44] Thus, it could possibly also prevent clogging of the nanopores. The structure of PEG is shown in Figure 3.5.

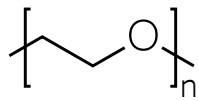

Figure 3.5: Chemical structure of PEG.

As already mentioned, the difficulty in preparation of polymer brushes using grafting-to is reaching a high enough grafting density. At low grafting density, PEG will tend to adopt a mushroom structure instead of the strongly stretched brush, reducing its anti-fouling properties.[37],[44] To circumvent this problem, grafting methods where the coil size is reduced are often employed, usually by choosing a less favourable solvent for the polymer during grafting. Grafting PEG with a thiol (-SH) functional group onto gold surfaces in 0.9 M Na_2SO_4 has been demonstrated to produce brushes whose height aligns with the Alexander - de Gennes "strongly stretched" brush.[44] More about PEG grafting on nanopores that was made for this thesis in Chapter 7.

Chapter 4

Experimental

This chapter describes the fabrication process for membranes and nanopores, as well as the ionic current measurements. The fabrication of nanochambers suitable for protein trapping is part of the developmental work of this thesis, and is detailed in Chapter 5. The grafting process for PEG polymer brushes is described in detail in Paper II and is summarised in Chapter 7.

4.1 Membrane fabrication

Nanopores were fabricated in 20 nm thick, free-standing SiN membranes (10x10 μm^2) supported on either 200 μm (Norcada) or 500 μm Si chips (5x5 mm^2). Nanochambers and nanopore arrays were also fabricated in free-standing SiN membranes on 500 μm Si chips (10x10 mm^2). The fabrication process for the 500 μm thick chips follows and is also summarised in Figure 4.1.

Before fabrication, the 4" Si wafer substrates were cleaned using a mixture of H_2O:NH_4OH:H_2O_2 (5:1:1 ratio) for 10 minutes at 80°C. This was followed by immersing the wafer for 1 minute in 2% HF solution, and then in H_2O:HCl:H_2O_2 (5:1:1 ratio) for 10 minutes at 80°C.

Low stress SiN was deposited on the Si wafer using low-pressure chemical vapour deposition (LP-CVD) at 820°C for 5 minutes (9 minutes for nanopore arrays). The SiN thickness was measured by ellipsometry to be 30 nm and 50 nm, respectively, for the different deposition times. The wafer was then spin-coated with a positive photoresist (S1813, Microposit) at 4000 RPM for 60 seconds, after which the wafer was baked at 120°C on a hotplate for 2 minutes. The membrane windows were defined through UV mask lithography, where 690 μm circles (770 μm for nanopore arrays) were patterned onto the wafer. Development was performed for 60 seconds (MF-319, Microposit).

Reactive ion etching (RIE) with CF_4/O_2 (4:1 volume flow, 50 W, 15 mTorr) was then used to etch through the exposed SiN for 5 minutes (9 minutes for nanopore arrays). This was followed by using an O_2 plasma (250 W, 500 mTorr) for 2 minutes to strip off the remaining photoresist. KOH was used to anisotropically etch through the wafer at 54.74° relative to the Si <100> plane. KOH etching (30% solution) was performed at 80°C for ~10 hours, until the

SiN membranes were left free-standing. At this point, the membranes for CBD and nanochamber fabrication were ∼10x10 μm^2 and ∼20 nm thick (due to thinning of the SiN during KOH etching), and for nanopore arrays ∼100x100 μm^2 and ∼40 nm thick.

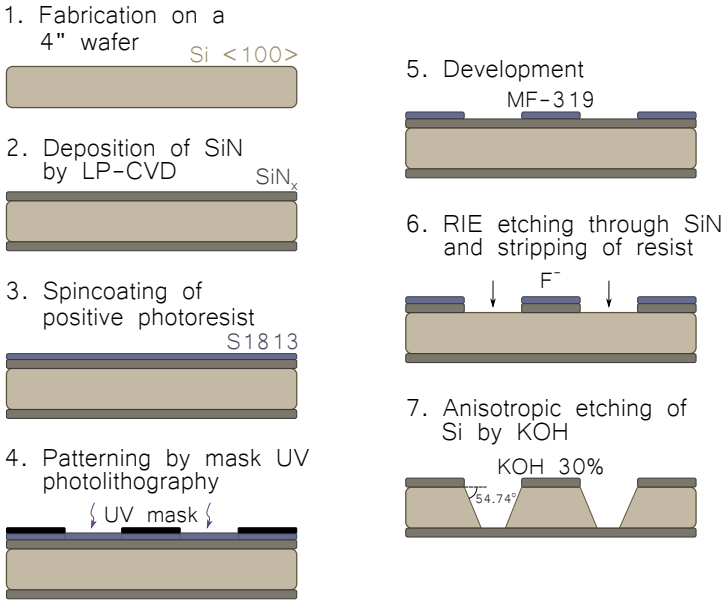

Figure 4.1: The membrane fabrication process.

4.2 Chemicals

All aqueous solutions were prepared using ASTM research-grade Type 1 ultra-filtered water (milliQ, 18.2 MΩcm). Nanopore fabrication and sensing experiments were carried out in 1 M KCl (AnalaR), 10 mM Tris, 1 mM EDTA (100x concentrate, Sigma Aldrich) buffered solution. Conditioning was performed in a 3.6 M LiCl (Sigma Aldrich) solution. The bulk conductivity of electrolyte solutions was measured using a multi-parameter meter (VWR pHenomenal MU6100L), approximately 10.7 S/m for 1 M KCl and around 16 S/m for 3.6 M LiCl at room temperature. For DNA sensing experiments, 1 nM of 3 kbp dsDNA (NoLimits DNA fragment, Thermo Fisher Scientific) was mixed with the buffer solution and introduced to the cis chamber of the flow cell. Similarly, for protein sensing experiments, 55 nM of $\beta-$galactosidase from *Aspergillus Oryzae* (Sigma Aldrich) was mixed with the buffer solution.

4.3 Nanopore fabrication by controlled breakdown

4.3.1 Experimental setup

Nanopores were fabricated in SiN membranes using the controlled breakdown (CBD) technique. The SPARK-E2 system, controlled with the NNi Nanopore Fabrication software (Northern Nanopore Instruments), was employed for this purpose. The chips were mounted in PEEK (polyether ether ketone) or plastic flow cells (Northern Nanopore Instruments). These flow cells were filled with electrolyte buffer and sealed with anti-evaporation caps equipped with Ag/AgCl electrodes as shown in Figure 4.2.

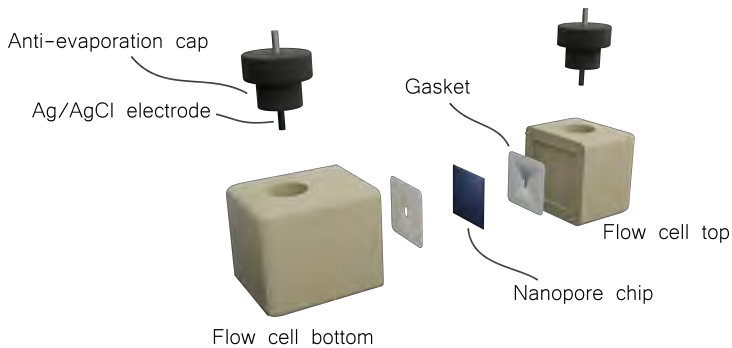

Figure 4.2: The components of the flow cell used for ion current measurements and CBD. The nanopore chip is sandwiched between two gaskets and mounted in the flow cell. The cell is subsequently filled with electrolyte buffer, and sealed using anti-evaporation caps equipped with Ag/AgCl electrodes.

4.3.2 Nanopore fabrication

Nanopore chips were cleaned using Piranha solution (3:1 mixture of H_2SO_4 and H_2O_2) for 20 minutes before nanopore fabrication. Prior to the fabrication process, an IV curve was recorded to assess the leakage current and ensure the absence of defects in the membrane. The fabrication involved sweeping the voltage from 0 to -5 V at a rate of -3 V/min. Once -5 V was reached, the sweep rate was reduced to -0.75 V/min. Simultaneously, the leakage current through the membrane was monitored, and the voltage application would be terminated upon the detection of a sudden current spike, indicative of pore formation. The termination threshold, calculated as an average over the last 50 current data points, was adjusted with an offset ranging from 10 to 150 nA. The voltage was continuously decreased until reaching the termination threshold. In cases where the maximum voltage of -18 V was reached before termination, the voltage was maintained at -18 V until fabrication occurred. A representative fabrication curve is presented in Figure 4.3. Nanopore fabrication was confirmed by recording another IV curve. A comparison between the IV

curves before and after fabrication is presented in Figure 4.4a). The equivalent pore size for these IV curves was determined using equation 2.2.

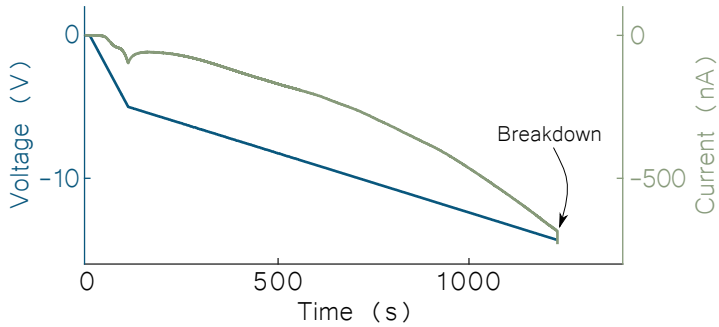

Figure 4.3: Measured current and applied voltage during fabrication of a nanopore using controlled breakdown.

4.3.3 Nanopore conditioning

After nanopore fabrication, a conditioning process was usually carried out. The primary purpose of conditioning was to enlarge the pore to the target size, although it also to achieve a more linear IV response. During conditioning, square voltage pulses of 4 seconds with alternating polarity were applied until the pore reached the desired size. Pulse amplitudes varied between experiments, typically ranging from 4 to 6 V, well below the breakdown voltage to prevent multiple pore formation. Figure 4.4b) shows an example of the applied voltage and measured current during a conditioning experiment. The final nanopore size was determined by recording another IV curve, also shown in the comparison in Figure 4.4a).

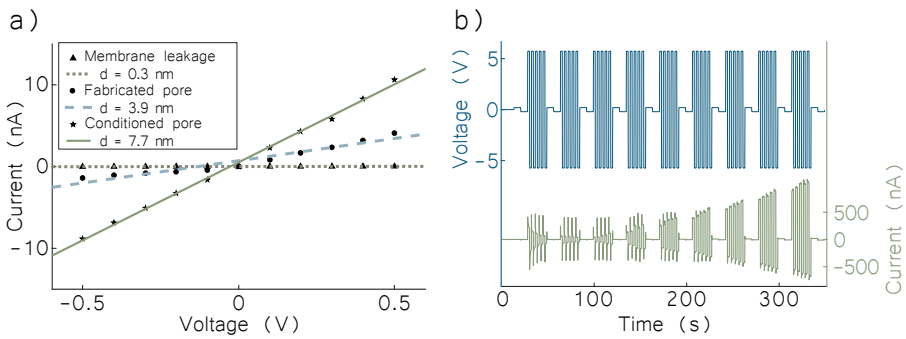

Figure 4.4: a) IV-curve of a nanopore before fabrication (membrane leakage), after fabrication and after conditioning. b) Current and voltage during conditioning of a nanopore.

4.4 Ion current measurements

The same flow cell as for CBD fabrication (Figure 4.2) was used, but placed inside a Faraday cage (Northern Nanopore Instruments). The current was recorded by the patch-clamp amplifier Axopatch 200B, and digitised by a Digidata 1550B (Molecular Devices). The experimental setup is shown in Figure 4.5. IV-curves were recorded using the WinWCP software, and current-time traces were recorded using the Axoscope software. Data analysis was performed using a custom-made MATLAB software, which is described more in detail in Chapter 6.

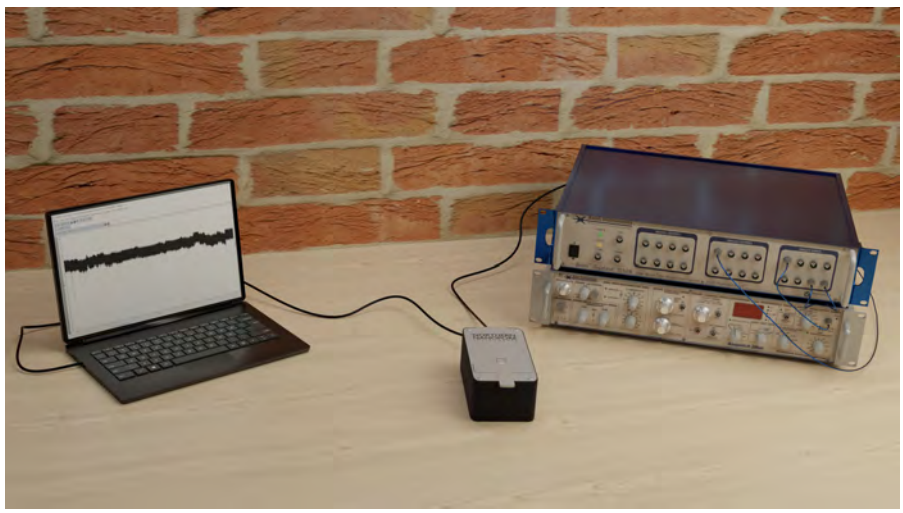

Figure 4.5: The experimental setup for ion current measurements, with the flow cell placed inside the Faraday cage, which is connected to the Axopatch 200B patch-clamp amplifier and the Digidata 1550B digitiser.

Chapter 5

Nanofabrication:

Nanoscale structures suitable for protein trapping and gating

To temporally resolve protein dynamics, one conceivable strategy involves confining proteins inside a nanostructure. This approach would enable long observation times of proteins, for example through fluorescence microscopy, without the risk of diffusion from the observation spot. Consequently, a crucial part of developing a platform for investigating single protein dynamics and interactions is the development of nanoscale gates and traps. This chapter provides an overview of the development and fabrication processes for two different types of nanostructures designed for protein trapping and gating.

5.1 Paper I: Nanopores for protein gating

My contribution to Paper I was the fabrication of membranes with nanopore arrays, that were used to demonstrate gating for proteins using thermoresponsive polymer brushes. This section outlines the fabrication process for nanopore arrays and provides a brief summary of their application in protein gating experiments.

5.1.1 Fabrication of nanopore arrays

The nanopore arrays were fabricated in 40 nm thick, free-standing SiN membranes (as described in Section 4.1). A schematic overview of the fabrication process for nanopore arrays is presented in Figure 5.1. The Si wafer with membranes underwent an initial cleaning step using H_2O:HCl:H_2O_2 (5:1:1 ratio) for 20 minutes at 80°C, in order to remove inorganic contaminants from the KOH etching process.

The lithography process started with spin-coating the membrane-side of the wafer with an adhesion promoter (Ti Prime, MicroChemicals) at 3000 RPM for 20 seconds. Subsequently, the wafer was baked in a furnace at 130°C for 10 minutes, to ensure proper adhesion of the resist (ma-N 2403, Microresist Technology), which was then spin coated at 3000 RPM for 60 seconds. Another round of baking followed in a furnace at 180°C for 10 minutes.

An array of circles (60 or 110 nm diameter, with either a 300 nm or 4 μm pitch) was patterned on each membrane using EBL (4 nm beam step size, 300 μm aperture, 2 nA beam current and a dose of 500 μC/cm^2 for dense arrays, 700 μC/cm^2 for sparse arrays). Subsequently, the resist was developed using developer ma-D 525 (Microresist Technology) for 60 seconds, creating an array of resist pillars on the membrane.

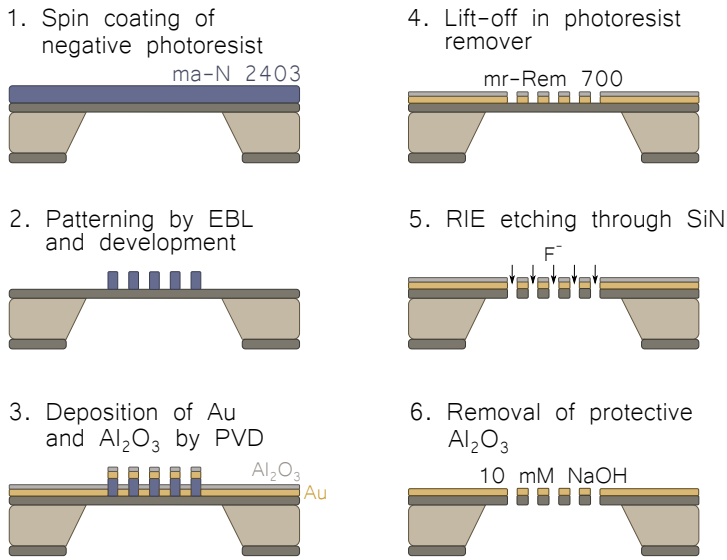

Figure 5.1: Schematic of the nanopore fabrication process.

The wafer was then prepared for Au deposition by subjecting it to 10 seconds of O_2 plasma (50 W, 250 mTorr, 80 sccm). This step was found to be crucial for removing residuals from the Ti prime adhesion promoter, which would otherwise interfere with the metal film adhesion. Physical vapour deposition (PVD) was then used to deposit 1 nm Cr (adhesion layer), 30 nm Au and 15 nm Al_2O_3 (protective layer) on the wafer. The outcome was an array of metal-covered resist pillars, which could be removed by a lift-off process where the wafer was mounted upside down in a Teflon holder in stirred and heated photoresist remover (mr-Rem 700) at 55°C for 15-30 minutes. This process left an array of holes in the metal film.

Reactive ion etching (RIE) with CF_4/O_2 (4:1 volume flow, 50 W, 15 mTorr) was then employed to etch through the exposed SiN for 9 minutes. The Al_2O_3 layer protects the Au during RIE, and can be removed afterwards by immersion in 10 mM NaOH for 45 minutes. This results in the formation of an array of nanopores in the free-standing membranes of SiN and Au. An SEM image of part of a nanopore array is shown in Figure 5.2a).

5.1.2 Protein gating in nanopores by thermo-responsive polymer brushes

The nanopore arrays served as a platform for demonstrating protein gating in experiments conducted by Justas Svirelis and Jesper Medin (affiliations in Paper I). In summary, poly(N-isopropylacrylamide) (PNIPAM) brushes were grafted onto the Au surface using a grafting-from approach. PNIPAM is a thermo-responsive polymer with a LCST at 32°C. Thus, by locally heating the nanopore membranes, the brush could be switched between an extended (gate closed) and collapsed (gate open) state, as illustrated in Figure 5.2c). Fluorescent bovine serum albumin (BSA) was introduced to one side of the nanopore membrane, and the fluorescence intensity was monitored on the opposite side of the membrane. The intensity increased only when the membrane was heated (Figure 5.2b), confirming that the fluorescent proteins could diffuse through the nanopores only when the PNIPAM brushes were in the collapsed state. The nanopores remained closed towards proteins when PNIPAM was in the extended state.

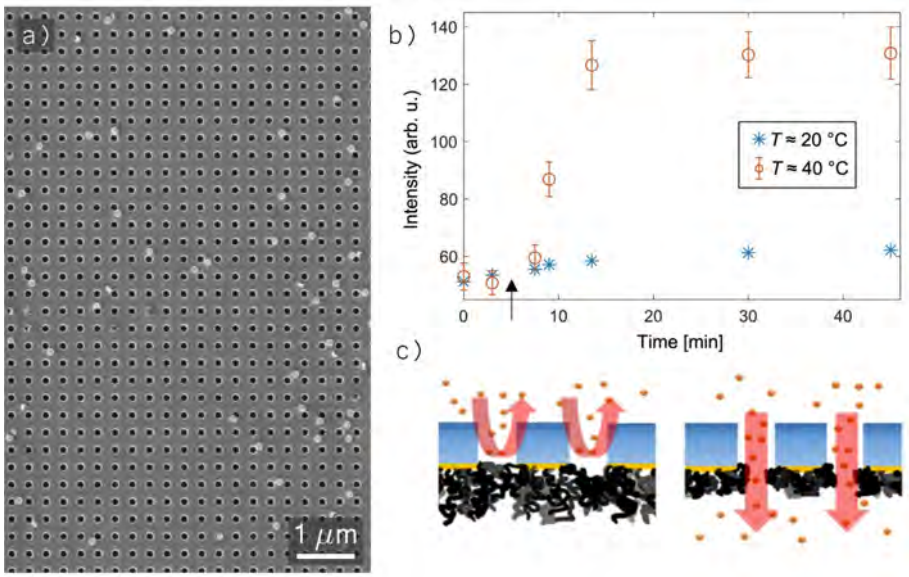

Figure 5.2: a) SEM image of a nanopore array. b) Fluorescence intensity over time showing that proteins can only pass through the nanopores when the membrane is heated. c) Schematic of the nanopores with brushes in an extended (gate closed) and collapsed (gate open) state.

5.2 Unpublished results: Nanochambers for protein trapping

While nanopore arrays were effective in demonstrating protein gating, they lack the capability for protein trapping. This section outlines the fabrication process for a novel nanochamber design aimed at capturing proteins. These chambers consist of a central cavity where proteins can potentially be confined. On each side of the cavity is a nanopore, serving as the "entrance" and "exit", as illustrated in Figure 5.3. While the nanochambers are yet to be used in protein trapping experiments, we present the demonstrated fabrication process including optical and electrical characterisation of the structure.

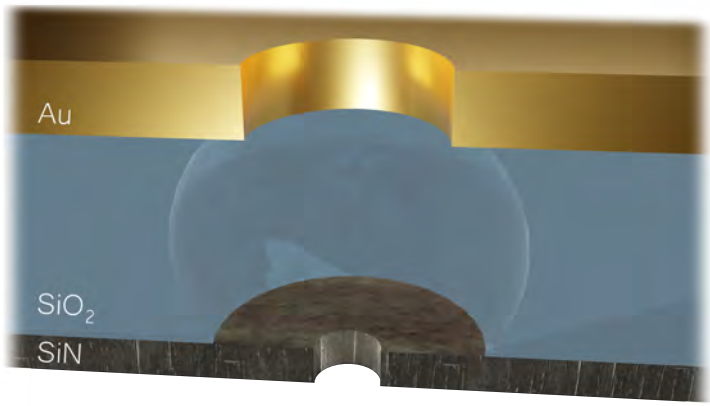

Figure 5.3: Illustration of a nanochamber in cross-section.

5.2.1 Nanochamber fabrication

The nanochamber fabrication process is to a large extent based on the fabrication of nanopore arrays. The entire process is summarised in Figure 5.4. To avoid redundancy, only the differences compared to nanopore arrays will be described here.

100 nm of SiO_2 was grown on 20 nm thick SiN membranes using atomic layer deposition (ALD). EBL was performed in the same way as for nanopore arrays, but patterning only one single circle with a diameter of 80-200 nm in the middle of each membrane (700 $\mu C/cm^2$ dose), to achieve one single nanochamber in each membrane. No Al_2O_3 was deposited on these membranes, as there is no RIE step in which the Au needs protection. The hole in the Au resulting after lift-off forms the nanochamber "exit" pore.

The chamber cavity was etched out in the SiO_2 layer by using buffered oxide etch (BOE 7:1) for 10-30 seconds. BOE 7:1 etches the SiO_2 more isotropically than RIE, with a theoretical etch rate of 80 nm/min.[49] The etch rates that we observed were significantly higher, corresponding to around 500 nm/min,

however with a considerable variation between different runs. The reason for this discrepancy is unknown, but is believed to be related to the SiO_2 quality.

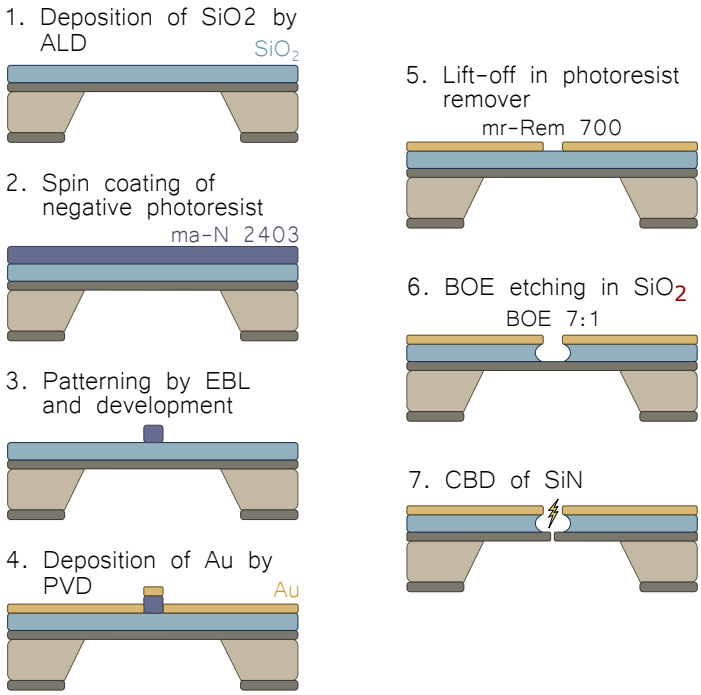

Figure 5.4: Schematic of the nanochamber fabrication process.

Finally, the nanochamber "entrance pore" was fabricated by CBD in the now exposed part of the SiN membrane at the bottom of the etched chamber. CBD was performed as described in Section 4.3. Note that the wafer had to be broken up into individual chips before this step, as the CBD process can only be performed on one membrane at the time. Figure 5.6a) shows the fabrication curve, featuring the characteristic current spike indicating nanopore fabrication.

SEM and TEM images of the nanochamber structure are shown in Figure 5.5. The Au pore and the etched SiO_2 cavity are visible in the images. For the TEM characterisation, the same fabrication process as described was performed but on TEM grids with 100x100 μm SiN windows (SiMPore). Instead of one single chamber on each membrane, an array of chambers with a 4 μm pitch was patterned. The TEM characterisation was performed by Takumi Sannomiya.

5.2.2 Electrical characterisation

The nanochambers were electrically characterised through the recording of IV curves both before and after CBD, as illustrated in Figure 5.6b). Notably, the pre-fabrication leakage current in nanochamber chips was relatively high, despite the small exposed SiN area ($\sim$ 500 times less than a full membrane).

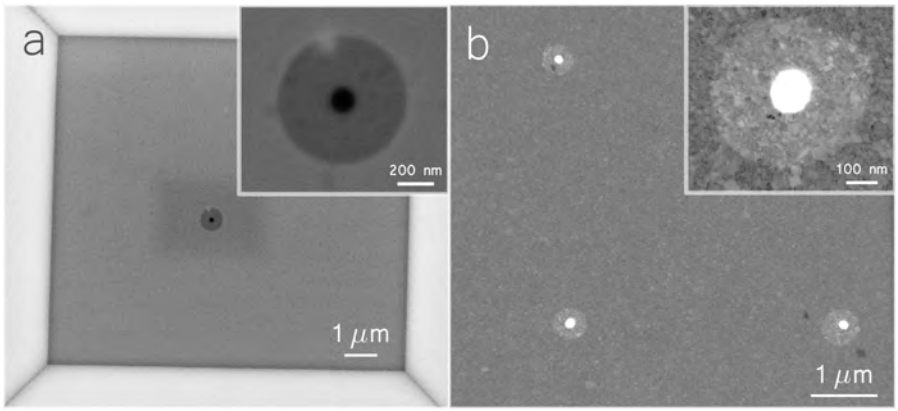

Figure 5.5: a) SEM image of a membrane with a single nanochamber. The inset shows a magnification of the chamber. b) TEM image of part of a membrane with a nanochamber array. The inset shows a magnification of one of the chambers.

While leakage through the SiO_2 covered part of the membrane is expected to be low due to the insulating properties of SiO_2, the observed high leakage current may be attributed to the potential etching of the exposed SiN during BOE etching. This process could lead to membrane thinning and/or the creation of small pores/defects in the SiN, as has been previously demonstrated.[50]

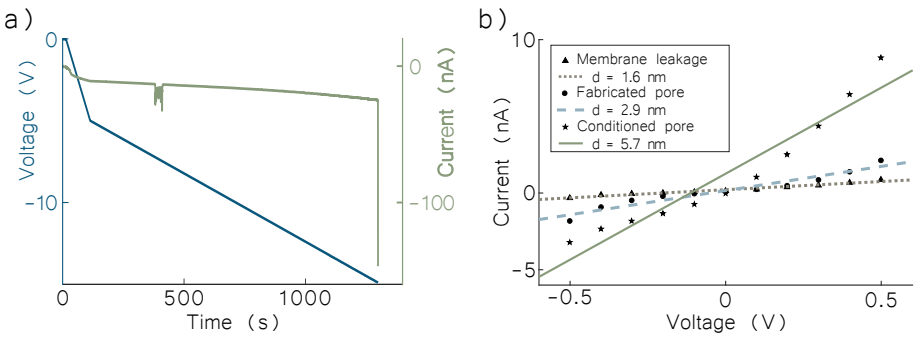

Figure 5.6: a) Current and voltage over time during CBD fabrication of a pore in the exposed SiN membrane in a nanochamber. b) IV-curves of the nanochamber before CBD, after CBD and after conditioning. The pore sizes given in the Figure are calculated using Equation 2.2.

The SiN pore is expected to be the dominating contribution to the combined nanostructure resistance due to its small size. For instance, the resistance of a 100 nm pore in a 30 nm thick membrane (corresponding to the EBL/RIE pore in the Au) is only about 1% of the resistance of a 5 nm pore in a 20 nm membrane. Thus, Equation 2.2 can still be used to estimate the size of the SiN pore. However, when the size difference is smaller, the resistance contribution from the Au pore is no longer negligible. Figure 5.6 also indicates that the

nanochamber exhibits rectifying IV characteristics. This may be related to the asymmetry of the geometry around the nanopore, with the cavity on one side of the pore.

Chapter 6

Data analysis:
Enabling high-voltage nanopore recordings

Nanopore sensing often encounters challenges related to noise in the current signal. This noise can originate from various sources, including low-frequency flicker noise and high-frequency capacitive noise[35],[36] While low-pass filtering is a common method to mitigate noise in nanopore data, it does not address issues such as an unstable or fluctuating baseline, something which becomes more pronounced at higher voltages. This may be a reason why most studies stay below 500 mV.

The instability of the baseline poses difficulties in reliable event detection and identification. Different event detection algorithms commonly employed in nanopore data analysis, such as threshold detection, cumulative sum or moving average[51],[52] may struggle with event detection in cases of severe baseline instability. In fact, even commercial software like Clampfit (Molecular Devices) and Nanolyzer (Northern Nanopore Instruments) were unable to correctly identify the events in high voltage experiments with fluctuating baselines. To overcome this issue and facilitate high-voltage (> 500 mV) nanopore recordings, I developed a MATLAB based software for nanopore data analysis. This software, in addition to conventional low-pass filtering, also features a high-pass filtering algorithm. This chapter provides a concise description of the algorithm and a showcases the software's application in an experiment with an unstable baseline.

6.1 Low- and high-pass filtering of nanopore data

As discussed in Section 2.6.1, the routinely performed low-pass filtering of nanopore recordings may result in information loss, if there are translocations above f_c. However, low-pass filtering often remains a necessity to distinguish any signal at all. An unstable baseline can be considered as a low-frequency variation in the signal. As the event data of interest is typically very high frequency (on the order of > 1 kHz), high-pass filtering can safely be applied without risking data loss.

The algorithm used in our nanopore data analysis software relies on the MATLAB Fast Fourier Transform (FFT), transforming the current-time trace into its frequency components. In the next step, the lowest frequency components, corresponding to baseline fluctuations, are eliminated from the data. The data is then inverse Fourier transformed (IFFT) back to the time domain, to regain the current trace, however with a stable baseline.

6.2 Data analysis example

Figure 6.1 presents an example of a current trace recorded at 900 mV (500 kHz sampling frequency, low-pass filtered at 10 kHz) with an unstable baseline. The resulting current trace after high-pass filtering at 100 Hz demonstrates the effectiveness of this approach in removing baseline fluctuations.

After filtering, events in the current trace can be accurately identified using a simple threshold detection algorithm. The threshold, set as a fixed number of standard deviations from the mean current, allows the registration of events whenever the current surpasses this threshold. The choice of threshold obviously impacts the number of detected events, where a balance is sought to avoid missing translocation events with a too high threshold or introducing "false positives" with a too low threshold. The threshold used in the present experiment is indicated in Figure 6.1.

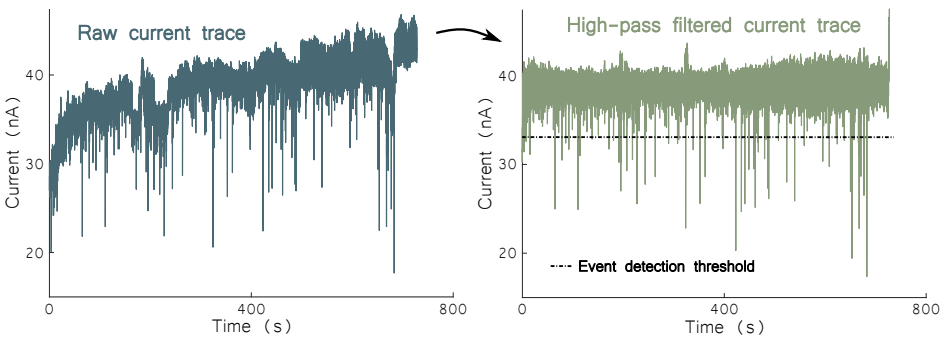

Figure 6.1: A current trace with an unstable baseline is high-pass filtered at 100 Hz to remove baseline fluctuations.

Chapter 7

Towards a voltage-gated nanopore

As demonstrated in Paper I and Chapter 5, the creation of a thermo-responsive gating system for proteins through the grafting of PNIPAM to nanopores has been established. However, exploring alternative macromolecular gating systems could introduce additional functionality. For instance, a voltage gated nanopore with ionic current readout would overcome the limitation of the thermally gated system, which cannot quantify the number of proteins passing through the gate in its open state. Except for the prospect of voltage gating, several other motivations drive the functionalisation of solid-state nanopores, addressing issues like pore clogging, reducing ionic current noise, enabling selective transport, and potentially facilitating the binding of analytes inside the pore through a functional surface coating tailored to specific analytes. In this chapter, we present a novel method for grafting PEG brushes on silica nanostructures (Paper II). The PEG functionalised nanopores are then characterised based on their ionic current response, and the translocation of dsDNA and β-galactosidase protein is demonstrated.

7.1 Paper II: Functionalised SiN nanopores

My contribution to Paper II involved functionalisation of SiN nanopores, and conducting the electrical characterisation of these pores. This work is presented here, including additional work performed after publication. However, first, let me provide a brief overview of the functionalisation protocol for PEG brushes on silica surfaces.

7.1.1 Grafting of PEG brushes to silica surfaces

The comprehensive functionalisation protocol for PEG brushes on silica surfaces is provided in Paper II, and the individual steps are illustrated in Figure 7.1. The method, developed by John Andersson (affiliations in Paper II), is based on aminopropylsilatrane (APS) click chemistry. The surface is functionalised in three simple steps. In summary, the method involves silanisation of the surface using APS, followed by a click-chemistry reaction with the crosslinker molecule

sulfo-SMCC. Thiol-PEG can then be grafted using the same protocol employed for the functionalisation of gold surfaces (grafting in 0.9 M Na_2SO_4), described in Section 3.3.1. The first two steps are completed within a few minutes, while the final PEG-grafting step can be conducted over 1 hour or left overnight. The method accommodates both an ex situ (immersion of the sample chip in solutions) and an in situ (injections of solutions into a flow cell) approach.

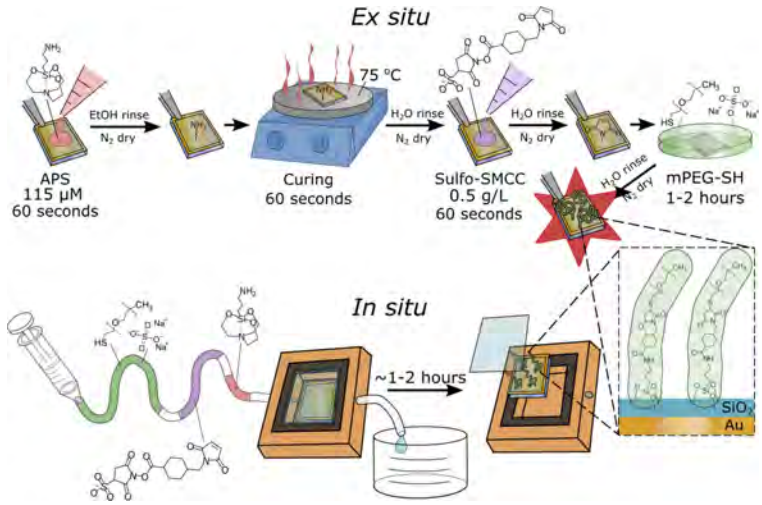

Figure 7.1: The functionalisation protocol for APS-SMCC-PEG on silica surfaces. Both the ex situ and in situ approaches are shown.

7.1.2 PEG grafting on SiN nanopores

The APS-SMCC-PEG functionalisation protocol was applied to modify the surface of nanopores fabricated by CBD, with sizes ranging from 7-35 nm. To confirm brush grafting inside the pores, the conductance was measured before and after functionalisation. In all cases, there was a significant decrease in conductance after functionalisation, as illustrated in Figure 7.2a) for a representative example. The mean conductance reduction for 2 kDa PEG grafting to nanopores was 85% (calculated over 23 pores). This reduction might appear high, considering the highly hydrated nature of the PEG brush ($\sim$ 80% on planar surfaces under physiological conditions), which implies a high ionic conductivity. However, the dense APS-SMCC layer ($\sim$ 4 nm) is assumed to have very limited conductivity. Additionally, the brush hydration inside nanopores is expected to be slightly lower than on planar surfaces.[47] This increased monomer density can be attributed to a combination of ionic strength (1 M KCl) and brush confinement inside the pore. The total brush exclusion height (including APS and SMCC) on a planar surface - representing the distance from the surface when proteins cannot penetrate the brush - was determined to be $\sim$ 13 nms. For most of the investigated pores, this suggests some compression of the brush inside the pore volume, however the brushes

can also stretch out in the free volume surrounding the pore.

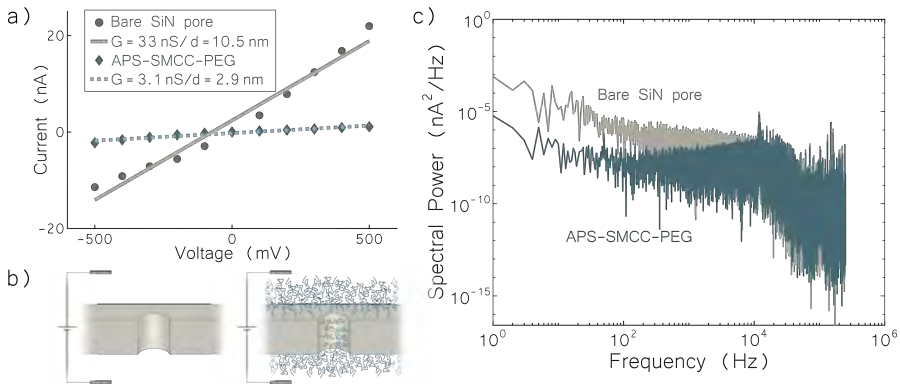

Figure 7.2: a) A typical IV curve before and after functionalisation, demonstrating a considerably reduced conductance of the pore. b) Schematic of a nanopore before and after PEG functionalisation. c) PSD of the nanopore current before and after functionalisation. The ionic current was recorded at 100 mV, 500 kHz sampling frequency and low-pass filtered at 10 kHz.

The nanopore noise characteristics before and after functionalisation were investigated by calculating the power spectral density (PSD). The PSD is calculated as the squared magnitude of the Fourier transform of the open-pore current, and is shown in Figure 7.2c) for the same nanopore as in Figure 7.2a). The modified pores often exhibited a reduction in the low-frequency $\frac{1}{f}$-noise. This low-frequency noise is often associated with nanopore surface properties. Thus, it is not unexpected that the surface modification of nanopores would influence the noise in this part of the frequency spectrum. The noise reduction observed can be attributed to a reduction in charge carriers and surface charge on the nanopore walls.

7.2 Unpublished results: Molecular translocation through functionalised nanopores

This section presents preliminary, unpublished results demonstrating voltage-gating of macromolecules. PEG brushes are known for their protein-repelling properties, and a previous study has shoen that PEG brushes on large (70-100 nm) pores act as an entropic barrier towards proteins.[6] However, the barrier properties of PEG under applied voltage has, to the best of my knowledge, not previously been investigated. To test this, 3 kbp dsDNA or β-galactosidase protein was added to the cis chamber of a APS-SMCC-PEG functionalised nanopore. No translocation events were detected below 500 mV for both the DNA and the protein. Interestingly, above 500 mV, translocation events could be clearly observed. Current traces for β-galactosidase in the transition region of 400-700 mV are shown in Figure 7.3a). It is apparent that the event frequency increases with applied voltage above the 500 mV threshold. A plot of the event

frequency versus voltage for both DNA and β-galactosidase is presented in Figure 7.3b).

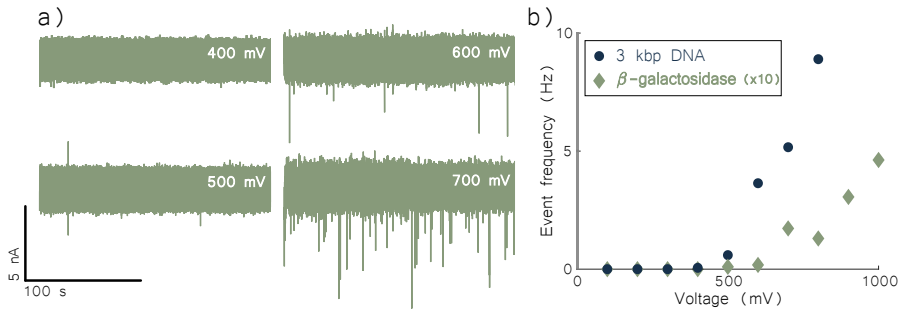

Figure 7.3: a) Current traces for 400-700 mV for β-galactosidase translocating an APS-SMCC-PEG (2 kDa) functionalised 16.6 nm pore (sampled at 500 kHz, low-pass filtered at 100 kHz, high-pass filtered at 100 Hz). b) Event frequency versus voltage for both β-galactosidase and 3 kbp dsDNA in APS-SMCC-PEG (2 kDa) functionalised pores. The pore size in the DNA experiment was 7.2 nm. Note that the event frequency for β-galactosidase is shown here x10.

As PEG brushes are uncharged, they should remain unaffected by the applied voltage. They would however be affected if there was an electroosmotic flow in the pore, but as the surface modification is expected to charge neutralise the surface, the electroosmotic flow should be negligible. Therefore, the observed voltage-gated behaviour is unlikely to be caused by a disruption in the PEG brush structure. Additionally, degrafting of PEG at high voltage can be ruled out, as the pore remained closed upon decreasing the voltage below the threshold. It is more plausible that voltage-gating occurs when the net force on the molecules becomes sufficiently strong to overcome the PEG barrier. In experiments conducted at high ionic strength (1 M KCl), the dominant force acting on both DNA and β-galactosidase (which has a negative net charge at pH 7) should be the electrophoretic force induced by the applied voltage. It is also interesting to note that the barrier towards translocation seems larger for β-galactosidase, as the event frequency was much lower compared to DNA even though the DNA concentration was lower (1 nM/55 nM). This also points towards the electrophoretic force as the main driving force, which is larger for DNA given the higher charge.

As discussed in Section 2.5, the capture rate for DNA in unmodified pores larger than $\sim$ 15 nm scales linearly with voltage. In the absence of a translocation barrier, diffusion becomes the rate-limiting step, leading to the formation of a depletion zone within the capture radius.[26] However, even though our modified pores exhibit zero translocation below the threshold voltage, charged molecules are still influenced by the electric field outside of the pore. In this cases, the presence of a strong barrier like PEG is likely to create a concentration zone where molecules, unable to escape the electric field, also cannot pass through the brush barrier. The verification of such a concentration zone is however still to be demonstrated.

Chapter 8

Conclusion and future work

This thesis has demonstrated some important progress towards the realisation of a nanoscale trap for single proteins. The fabrication process for a nanochamber with dimensions suitable for trapping single proteins has been developed. The next step would be the integration of this nanostructure with polymer brush surface functionalisation. As the nanochamber consists of both gold and silica surfaces, there is potential for material-specific functionalisation. This allows the "exit pore" to be modified with a unique surface coating distinct to the rest of the structure. For instance, envisioning a combination of grafting-from and grafting-to approaches could yield a system exhibiting both voltage- and thermal gating. The ultimate objective is to successfully trap proteins within the nanochamber. Initially, translocations through the nanostructure should be tested, before proceeding to protein entrapment. The subsequent study of trapped proteins are likely to utilise fluorescence based techniques in a confocal microscope. Thus, the integration of optical measurements with the electrical nanopore sensing is crucial for enabling simultaneous readout.

Furthermore, this thesis highlights the successful functionalisation of nanopore sensors with polymer brushes, opening up for many new possibilities in nanopore sensing technology. Applications range from selective sensing and membrane transport to probing binding kinetics with ionic current readout. The observed voltage-gated capture behaviour also warrants further investigation, offering insights into the physics governing molecular transport through nanopores. Some areas for exploration include understanding how the threshold voltage correlates with pore size, polymer length and to extend the study to different proteins.

Acknowledgements

Firstly, I would like to express my sincere gratitude to the European Research Council for funding this project. The work was carried out at the Division of Applied Chemistry, Department of Chemistry and Chemical Engineering, Chalmers University of Technology, and in part at Myfab Chalmers.

This thesis would not have been possible without the guidance and support from my supervisor Andreas Dahlin. I am thankful for the opportunity to conduct my research within his group, which has helped me develop both as a researcher and as a person. I would also like to acknowledge my co-supervisor Fredrik Höök, my examiner Martin Andersson and my director of studies Ergang Wang. Many thanks also to all the colleagues at the division and to past and present members of the group. Special thanks to John for providing invaluable support and knowledge, and for showing me how to save important time in the cleanroom, without which this thesis never would have been completed on time. A special thanks also to Bagus, for taking on the cumbersome task of teaching a physicist proper lab etiquette. I also want to thank Gaurav for introducing me to the world of nanopore sensors, and to the team at Northern Nanopore, for always taking their time to share their experiences and knowledge about the intricacies of ion currents. I would also like to extend my sincere gratitude to my high school physics teacher Marcus Erhagen, who inspired me to study physics at university, and to Björn Wickman, my supervisor during undergraduate and masters studies, for having an influential role in my early academic career and my decision to pursue a PhD.

I also would not have been able to write this thesis without all the love and support from friends and family. Thanks to Ehsan for all the laughs we shared as office mates, and to Oskar for being a great friend throughout all these years, I look forward to sharing the rest of our PhD journeys. I am also thankful to all my friends outside of Chalmers, for providing distractions and emotional support when needed, for board game nights and evenings at the dog training club, and for understanding when I don't always reach out. To my parents, for their encouragement and for always believing in me. And last but not least, to the one who is always by my side, and who reminds me to take a break from work sometimes - my dog, Chili.

Julia Järlebark
Hisings Backa, January 2024

Bibliography

[1] R. Feynman, *There is Plenty of Room at the Bottom*, 1959.

[2] S. Bayda, M. Adeel, T. Tuccinardi, M. Cordani and F. Rizzolio, *The history of nanoscience and nanotechnology: From chemical-physical applications to nanomedicine*, 2020. doi: 10.3390/molecules25010112.

[3] M. Brucale, B. Schuler and B. Samorì, "Single-molecule studies of intrinsically disordered proteins," *Chemical Reviews*, vol. 114, no. 6, pp. 3281–3317, Mar. 2014, issn: 15206890. doi: 10.1021/cr400297g.

[4] C. Soto and S. Pritzkow, "Protein misfolding, aggregation, and conformational strains in neurodegenerative diseases," *Nature Neuroscience*, vol. 21, no. 10, pp. 1332–1340, Oct. 2018, issn: 15461726. doi: 10.1038/s41593-018-0235-9.

[5] C. Y. Lin, R. Fotis, Z. Xia *et al.*, "Ultrafast Polymer Dynamics through a Nanopore," *Nano Letters*, vol. 22, no. 21, pp. 8719–8727, Nov. 2022, issn: 15306992. doi: 10.1021/acs.nanolett.2c03546.

[6] G. Emilsson, K. Xiong, Y. Sakiyama *et al.*, "Polymer brushes in solid-state nanopores form an impenetrable entropic barrier for proteins," *Nanoscale*, vol. 10, no. 10, pp. 4663–4669, Mar. 2018, issn: 20403372. doi: 10.1039/c7nr09432a.

[7] G. Emilsson, Y. Sakiyama, B. Malekian *et al.*, "Gating Protein Transport in Solid State Nanopores by Single Molecule Recognition," *ACS Central Science*, vol. 4, no. 8, pp. 1007–1014, Aug. 2018, issn: 23747951. doi: 10.1021/acscentsci.8b00268.

[8] J. O. Zoppe, N. C. Ataman, P. Mocny, J. Wang, J. Moraes and H. A. Klok, "Surface-Initiated Controlled Radical Polymerization: State-of-the-Art, Opportunities, and Challenges in Surface and Interface Engineering with Polymer Brushes," *Chemical Reviews*, vol. 117, no. 3, pp. 1105–1318, Feb. 2017, issn: 15206890. doi: 10.1021/acs.chemrev.6b00314.

[9] M. D. Graham, "The Coulter Principle: A history," *Cytometry Part A*, vol. 101, no. 1, pp. 8–11, Jan. 2022, issn: 15524930. doi: 10.1002/cyto.a.24505.

[10] E. Neher and B. Sakmann, "Single-channel currents recorded from membrane of denervated frog muscle fibres," *Nature*, vol. 260, pp. 799–801, Apr. 1976.

[11] M. Dallas and D. Bell, Eds., *Patch Clamp Electro-physiology*. Springer Protocols, 2021. [Online]. Available: http://www.springer.com/series/7651.

[12] D. Deamer, M. Akeson and D. Branton, "Three decades of nanopore sequencing," *Nature Biotechnology*, vol. 34, no. 5, pp. 518–524, May 2016, issn: 15461696. doi: 10.1038/nbt.3423.

[13] Y. Wu and J. J. Gooding, "The application of single molecule nanopore sensing for quantitative analysis," *Chemical Society Reviews*, vol. 51, no. 10, pp. 3862–3885, May 2022, issn: 14604744. doi: 10.1039/d1cs00988e.

[14] L. Xue, H. Yamazaki, R. Ren, M. Wanunu, A. P. Ivanov and J. B. Edel, "Solid-state nanopore sensors," *Nature Reviews Materials*, vol. 5, no. 12, pp. 931–951, Dec. 2020, issn: 20588437. doi: 10.1038/s41578-020-0229-6.

[15] J. J. Kasianowicz, E. Brandin, D. Branton and D. W. Deamer, "Characterization of individual polynucleotide molecules using a membrane channel," *Biophysics*, vol. 93, pp. 13 770–13 773, 1996. [Online]. Available: https://www.pnas.org.

[16] C. Dekker, "Solid-state nanopores," *Nature Nanotechnology*, vol. 2, pp. 209–215, 2007. [Online]. Available: www.nature.com/naturenanotechnology.

[17] C. Wen, S. Zeng, S. Li, Z. Zhang and S. L. Zhang, "On Rectification of Ionic Current in Nanopores," *Analytical Chemistry*, vol. 91, no. 22, pp. 14 597–14 604, Nov. 2019, issn: 15206882. doi: 10.1021/acs.analchem.9b03685.

[18] B. Malekian, K. Xiong, E. S. Kang *et al.*, "Optical properties of plasmonic nanopore arrays prepared by electron beam and colloidal lithography," *Nanoscale Advances*, vol. 1, no. 11, pp. 4282–4289, 2019, issn: 25160230. doi: 10.1039/c9na00585d.

[19] Y. C. Chou, P. Masih Das, D. S. Monos, D. S. Monos and M. Drndić, "Lifetime and Stability of Silicon Nitride Nanopores and Nanopore Arrays for Ionic Measurements," *ACS Nano*, vol. 14, no. 6, pp. 6715–6728, Jun. 2020, issn: 1936086X. doi: 10.1021/acsnano.9b09964.

[20] H. Kwok, K. Briggs and V. Tabard-Cossa, "Nanopore fabrication by controlled dielectric breakdown," *PLoS ONE*, vol. 9, no. 3, Mar. 2014, issn: 19326203. doi: 10.1371/journal.pone.0092880.

[21] H. Kwok, M. Waugh, J. Bustamante, K. Briggs and V. Tabard-Cossa, "Long passage times of short ssDNA molecules through metallized nanopores fabricated by controlled breakdown," *Advanced Functional Materials*, vol. 24, no. 48, pp. 7745–7753, Dec. 2014, issn: 16163028. doi: 10.1002/adfm.201402468.

[22] S. W. Kowalczyk, A. Y. Grosberg, Y. Rabin and C. Dekker, "Modeling the conductance and DNA blockade of solid-state nanopores," *Nanotechnology*, vol. 22, no. 31, Aug. 2011, issn: 09574484. doi: 10.1088/0957-4484/22/31/315101.

[23] J. Hall, "Access Resistance of a Small Circular Pore," *The Journal of General Physiology*, vol. 66, pp. 531–532, Jun. 1975.

[24] D. L. Harame, L. J. Bousse, J. D. Shott and J. D. Meindl, "Ion-Sensing Devices with Silicon Nitride and Borosilicate Glass Insulators," *Transactions on Electron Devices*, vol. 34, no. 8, pp. 1700–1707, Aug. 1987.

[25] M. Firnkes, D. Pedone, J. Knezevic, M. Döblinger and U. Rant, "Electrically facilitated translocations of proteins through silicon nitride nanopores: Conjoint and competitive action of diffusion, electrophoresis, and electroosmosis," *Nano Letters*, vol. 10, no. 6, pp. 2162–2167, Jun. 2010, issn: 15306984. doi: 10.1021/nl100861c.

[26] P. Chen, J. Gu, E. Brandin, Y. R. Kim, Q. Wang and D. Branton, "Probing single DNA molecule transport using fabricated nanopores," *Nano Letters*, vol. 4, no. 11, pp. 2293–2298, Nov. 2004, issn: 15306984. doi: 10.1021/nl048654j.

[27] C. Wen and S. L. Zhang, "On current blockade upon analyte translocation in nanopores," *Journal of Applied Physics*, vol. 129, no. 6, Feb. 2021, issn: 10897550. doi: 10.1063/5.0035113.

[28] H. Chang, F. Kosari, G. Andreadakis, M. A. Alam, G. Vasmatzis and R. Bashir, "DNA-mediated fluctuations in ionic current through silicon oxide nanopore channels," *Nano Letters*, vol. 4, no. 8, pp. 1551–1556, Aug. 2004, issn: 15306984. doi: 10.1021/nl049267c.

[29] R. M. Smeets, U. F. Keyser, D. Krapf, M. Y. Wu, N. H. Dekker and C. Dekker, "Salt dependence of ion transport and DMA translocation through solid-state nanopores," *Nano Letters*, vol. 6, no. 1, pp. 89–95, Jan. 2006, issn: 15306984. doi: 10.1021/nl052107w.

[30] A. Gubbiotti, M. Baldelli, G. Di Muccio, P. Malgaretti, S. Marbach and M. Chinappi, "Electroosmosis in nanopores: computational methods and technological applications," *Advances in Physics: X*, vol. 7, no. 1, 2022, issn: 23746149. doi: 10.1080/23746149.2022.2036638.

[31] S. Van Dorp, U. F. Keyser, N. H. Dekker, C. Dekker and S. G. Lemay, "Origin of the electrophoretic force on DNA in solid-state nanopores," *Nature Physics*, vol. 5, no. 5, pp. 347–351, 2009, issn: 17452481. doi: 10.1038/nphys1230.

[32] L. Zhan, Y. Zhang, W. Si, J. Sha and Y. Chen, "Detection and Separation of Single-Stranded DNA Fragments Using Solid-State Nanopores," *Journal of Physical Chemistry Letters*, vol. 12, no. 28, pp. 6469–6477, Jul. 2021, issn: 19487185. doi: 10.1021/acs.jpclett.1c01163.

[33] M. Wanunu, W. Morrison, Y. Rabin, A. Y. Grosberg and A. Meller, "Electrostatic focusing of unlabelled DNA into nanoscale pores using a salt gradient," *Nature Nanotechnology*, vol. 5, no. 2, pp. 160–165, 2010, issn: 17483395. doi: 10.1038/nnano.2009.379.

[34] N. Mohanty, *Signal Processing*. Dordrecht: Springer Netherlands, 1988, isbn: 978-94-011-7046-8. doi: 10.1007/978-94-011-7044-4. [Online]. Available: http://link.springer.com/10.1007/978-94-011-7044-4.

[35] R. M. Smeets, U. F. Keyser, N. H. Dekker and C. Dekker, "Noise in solid-state nanopores," *Proceedings of the National Academy of Sciences of the United States of America*, vol. 105, no. 2, pp. 417–421, Jan. 2008, issn: 00278424. doi: 10.1073/pnas.0705349105.

[36] V. Tabard-Cossa, "Instrumentation for Low-Noise High-Bandwidth Nanopore Recording," in 2013. doi: 10.1016/B978-1-4377-3473-7.00003.

[37] A. Hucknall, S. Rangarajan and A. Chilkoti, "In pursuit of zero: Polymer brushes that resist the adsorption of proteins," *Advanced Materials*, vol. 21, no. 23, pp. 2441–2446, Jun. 2009, issn: 09359648. doi: 10.1002/adma.200900383.

[38] O. M. Eggenberger, C. Ying and M. Mayer, "Surface coatings for solid-state nanopores," *Nanoscale*, vol. 11, no. 42, pp. 19 636–19 657, Nov. 2019, issn: 20403372. doi: 10.1039/c9nr05367k.

[39] M. Salehirozveh, A. K. Kure Larsen, M. Stojmenovic, F. Thei and M. Dong, "In-situ PLL-g-PEG Functionalized Nanopore for Enhancing Protein Characterization," *Chemistry - An Asian Journal*, vol. 18, no. 17, Sep. 2023, issn: 1861471X. doi: 10.1002/asia.202300515.

[40] J. Roman, N. Jarroux, G. Patriarche *et al.*, "Functionalized Solid-State Nanopore Integrated in a Reusable Microfluidic Device for a Better Stability and Nanoparticle Detection," *ACS Applied Materials and Interfaces*, vol. 9, no. 48, pp. 41 634–41 640, Dec. 2017, issn: 19448252. doi: 10.1021/acsami.7b14717.

[41] Z. Tang, B. Lu, Q. Zhao, J. Wang, K. Luo and D. Yu, "Surface modification of solid-state nanopores for sticky-free translocation of single-stranded DNA," *Small*, vol. 10, no. 21, pp. 4332–4339, Nov. 2014, issn: 16136829. doi: 10.1002/smll.201401091.

[42] S. Koltzenburg, M. Maskos and O. Nuyken, *Polymer Chemistry*. 2017.

[43] G. J. Fleer, M. A. C. Stuart, J. M. H. M. Scheutjens, T. Cosgrove and B. Vincent, *Polymers at Interfaces*. Springer Netherlands, 1998. doi: 10.1007/978-94-011-2130-9.

[44] G. Emilsson, R. L. Schoch, L. Feuz, F. Höök, R. Y. Lim and A. B. Dahlin, "Strongly stretched protein resistant poly(ethylene glycol) brushes prepared by grafting-to," *ACS Applied Materials and Interfaces*, vol. 7, no. 14, pp. 7505–7515, Apr. 2015, issn: 19448252. doi: 10.1021/acsami.5b01590.

[45] W. L. Chen, R. Cordero, H. Tran and C. K. Ober, "50th Anniversary Perspective: Polymer Brushes: Novel Surfaces for Future Materials," *Macromolecules*, vol. 50, no. 11, pp. 4089–4113, Jun. 2017, issn: 15205835. doi: 10.1021/acs.macromol.7b00450.

[46] S. T. Milner, T. A. Witten and M. E. Cates, "Theory of the Grafted Polymer Brush," *Macromolecules*, vol. 21, no. 8, pp. 2610–2619, 1988. [Online]. Available: https://pubs.acs.org/sharingguidelines.

[47] M Manghi, M Aubouy, C Gay, C Ligoure and G. Théorie, "Inwardly curved polymer brushes: concave is not like convex," *Eur. Phys. J. E*, vol. 5, pp. 519–530, 2001.

[48] M. Y. Laktionov, E. B. Zhulina, R. P. Richter and O. V. Borisov, "Polymer brush in a nanopore: Effects of solvent strength and macromolecular architecture studied by self-consistent field and scaling theory," *Polymers*, vol. 13, no. 22, Nov. 2021, issn: 20734360. doi: 10.3390/polym13223929.

[49] P. Stevic, "BOE / HF-Silicon dioxide Etching Standard Operating Procedure," Tech. Rep., 2018. [Online]. Available: https://www.sigmaaldrich.com/catalog/product/mm/100335?lang=en&region=NL.

[50] Z. Xia, A. Scott, R. Keneipp *et al.*, "Silicon Nitride Nanopores Formed by Simple Chemical Etching: DNA Translocations and TEM Imaging," *ACS Nano*, vol. 16, no. 11, pp. 18 648–18 657, Nov. 2022, issn: 1936086X. doi: 10.1021/acsnano.2c07240.

[51] J. H. Forstater, K. Briggs, J. W. Robertson *et al.*, "MOSAIC: A modular single-molecule analysis interface for decoding multistate nanopore data," *Analytical Chemistry*, vol. 88, no. 23, pp. 11 900–11 907, Dec. 2016, issn: 15206882. doi: 10.1021/acs.analchem.6b03725.

[52] C. Plesa and C. Dekker, "Data analysis methods for solid-state nanopores," *Nanotechnology*, vol. 26, no. 8, Feb. 2015, issn: 13616528. doi: 10.1088/0957-4484/26/8/084003.